H^+ Transport by K^+ EXCHANGE ANTIPORTER3 Promotes Photosynthesis and Growth in Chloroplast ATP Synthase Mutants[1][OPEN]

Viviana Correa Galvis,[a] Deserah D. Strand,[a] Michaela Messer,[a] Wolfram Thiele,[a] Stephanie Bethmann,[b] Dennis Hübner,[a] Michal Uflewski,[a] Elias Kaiser,[a,2] Beata Siemiatkowska,[a] Bethan A. Morris,[a] Szilvia Z. Tóth,[c] Mutsumi Watanabe,[a] Franziska Brückner,[a] Rainer Höfgen,[a] Peter Jahns,[b] Mark Aurel Schöttler,[a] and Ute Armbruster[a,3,4]

[a]Max Planck Institute of Molecular Plant Physiology, Wissenschaftspark Golm, Am Mühlenberg 1, 14476 Potsdam, Germany

[b]Institute of Plant Biochemistry, Heinrich-Heine-University Düsseldorf, Universitätsstr. 1, D-40225 Düsseldorf, Germany

[c]Institute of Plant Biology, Biological Research Centre, Szeged, Temesvári krt 62, H-6726 Szeged, Hungary

ORCID IDs: 0000-0002-8092-9148 (V.C.G.); 0000-0002-6179-7901 (D.D.S); 0000-0003-2604-9876 (M.M.); 0000-0002-9081-9604 (E.K.); 0000-0003-3419-829X (S.Z.T.); 0000-0001-8590-9800 (R.H.); 0000-0002-5340-1153 (P.J.); 0000-0003-3210-0260 (M.A.S.); 0000-0002-8814-8207 (U.A.).

The composition of the thylakoid proton motive force (pmf) is regulated by thylakoid ion transport. Passive ion channels in the thylakoid membrane dissipate the membrane potential ($\Delta\psi$) component to allow for a higher fraction of pmf stored as a proton concentration gradient (ΔpH). K^+/H^+ antiport across the thylakoid membrane via K+ EXCHANGE ANTIPORTER3 (KEA3) instead reduces the ΔpH fraction of the pmf. Thereby, KEA3 decreases nonphotochemical quenching (NPQ), thus allowing for higher light use efficiency, which is particularly important during transitions from high to low light. Here, we show that in the background of the Arabidopsis (*Arabidopsis thaliana*) chloroplast (cp)ATP synthase assembly mutant *cgl160*, with decreased cpATP synthase activity and increased pmf amplitude, KEA3 plays an important role for photosynthesis and plant growth under steady-state conditions. By comparing *cgl160* single with *cgl160 kea3* double mutants, we demonstrate that in the *cgl160* background loss of KEA3 causes a strong growth penalty. This is due to a reduced photosynthetic capacity of *cgl160 kea3* mutants, as these plants have a lower lumenal pH than *cgl160* mutants, and thus show substantially increased pH-dependent NPQ and decreased electron transport through the cytochrome b_6f complex. Overexpression of *KEA3* in the *cgl160* background reduces pH-dependent NPQ and increases photosystem II efficiency. Taken together, our data provide evidence that under conditions where cpATP synthase activity is low, a KEA3-dependent reduction of ΔpH benefits photosynthesis and growth.

In plants, photosynthesis occurs in specialized organelles, the chloroplasts. Light energy is collected by light harvesting complexes in the thylakoid membrane, and the resulting excitation energy is transferred to two photosystems, PSI and PSII, where it induces charge separations. These drive electron transfer reactions from water to $NADP^+$ along the linear electron transport chain, including plastoquinone (PQ), the cytochrome b_6f (Cyt b_6f) complex, and the soluble, lumen-localized electron carrier plastocyanin (PC). Water oxidation at PSII releases protons into the thylakoid lumen. Additionally, the electron transfer reactions from PSII to Cyt b_6f are coupled to the translocation of protons from the stroma into the thylakoid lumen via the PQ pool. The accumulation of protons in the thylakoid lumen results in a charge difference, leading to a membrane potential ($\Delta\Psi$), and a proton concentration gradient (ΔpH) across the thylakoid membrane (reviewed by Armbruster et al., 2017). Both $\Delta\Psi$ and ΔpH contribute to the proton motive force (pmf) that drives protons through the chloroplast (cp)ATP synthase, providing the energy required for ATP synthesis (reviewed by Allen, 2002).

While both components of the pmf are energetically equivalent, the ΔpH plays an additional role in the feedback regulation of photosynthetic light capture and electron transport in response to light stress or other environmental factors that influence excitation pressure. With rising excitation levels and electron transport rates, downstream carbon fixation and other metabolic processes become limiting, which results in an increased acidification of the thylakoid lumen. Above certain thresholds, the proton concentration induces two processes that lead to the feedback down-regulation of light harvesting and electron transport, respectively. First, protonation of the thylakoid PsbS protein at the lumenal side occurs below a lumen pH of 6.8 (Takizawa et al., 2007). This in turn leads to the rearrangement of PSII supercomplexes and an increase in the thermal dissipation of absorbed light energy

(Li et al., 2004; Correa-Galvis et al., 2016; Sacharz et al., 2017). This so-called energy-dependent quenching (qE) component of nonphotochemical quenching (NPQ) is further sustained by zeaxanthin production via the low pH-activated violaxanthin de-epoxidase (VDE) localized in the lumen of land plants (Hager, 1969; Niyogi et al., 1998). Second, when lumen pH decreases below 6.5, plastoquinol (PQH_2) oxidation at Cyt b_6f is slowed down, a process referred to as "photosynthetic control" (Stiehl and Witt, 1969; Tikhonov et al., 1981; Nishio and Whitmarsh, 1993). At a lumen pH of 5.7, Cyt b_6f turnover is decreased 5- to 10-fold compared with its maximum rate (Nishio and Whitmarsh, 1993; Takizawa et al., 2007). This is because PQH_2 oxidation, which releases protons into the lumen, becomes thermodynamically less favorable. Additionally, amino acid residues at the lumenal side of Cyt b_6f, which receive the protons from PQH_2, are partially protonated at low lumenal pH (reviewed by Tikhonov, 2014).

The proton conductivity of the cpATP synthase is reduced in response to environmental factors that limit downstream metabolism, such as low CO_2 and drought stress (Kanazawa and Kramer, 2002; Kohzuma et al., 2009). Low conductivity results in the build-up of high pmf and thereby activates feedback down-regulation of photosynthesis. For wild watermelon (*Citrullus lanatus*) plants under drought stress conditions, it has been shown that the decreased cpATP synthase activity correlates with a strong down-regulation of its content and that a large fraction of the resulting high pmf is stored as $\Delta\Psi$ (Kohzuma et al., 2009). The same has been reported for tobacco (*Nicotiana benthamiana*) and Arabidopsis (*Arabidopsis thaliana*) mutants with constitutively lower cpATP synthase conductivity, due to decreased levels or activities, which have high pmf and a large fraction of it stored as $\Delta\Psi$ (Rott et al., 2011; Fristedt et al., 2015; Davis et al., 2016). Whether and how this adjusted pmf composition affects photosynthesis and growth remains to be determined.

Thylakoid ion transport proteins influence the composition of the pmf that is stored as $\Delta\Psi$ and ΔpH and thus the capacity of the pmf to regulate light harvesting and electron transport. Passive ion channels allow for the dissipation of the $\Delta\Psi$ component of the pmf. Because the proton buffering capacity of the lumen is high, $\Delta\Psi$ dissipation by these ion channels has been proposed to be required for storage of pmf as ΔpH (Kramer et al., 2003). In early experiments on isolated thylakoids, it was shown that proton translocation into the lumen is accompanied by counter-ion fluxes (Hind et al., 1974). These mainly consist of Cl^-, Mg^{2+}, and potentially K^+. Only the VOLTAGE-DEPENDENT CL− CHANNEL1 (VCCN1) protein localized in the thylakoids has been identified so far (Duan et al., 2016; Herdean et al., 2016). Lack of this protein in the *vccn1* mutant causes increased pmf, a larger fraction of pmf stored as $\Delta\Psi$, and slower induction of NPQ. The opposite behavior was observed when VCCN1 was overexpressed (Herdean et al., 2016). These data suggest that Cl^- plays a role in dissipating the membrane potential component of the pmf via VCCN1 in order to allow for a faster induction of thermal dissipation.

While counter ion movement is likely not restricted to Cl^-, the molecular nature of other counter-ion channels remains unknown: for example, the TWO-PORE K^+ CHANNEL 3 (TPK3) was found to localize to the thylakoid membrane and have a function comparable with VCCN1 in pmf modulation by mediating K^+ flux (Carraretto et al., 2013). However, a recent study (Höhner et al., 2019) supports earlier localization experiments, which showed TPK3 to exclusively reside in the tonoplast (Voelker et al., 2006; Dunkel et al., 2008). Additionally, a line with a transfer-DNA insertion in the *TPK3* locus did not show any differences in pmf composition and NPQ induction, strongly suggesting that TPK3 does not mediate transthylakoid K^+ flux (Höhner et al., 2019). Thus, the molecular nature of other $\Delta\Psi$-dissipating ion channels besides VCCN1 remains to be elucidated. Recently, it was shown that high $\Delta\Psi$ favors charge recombination in PSII (Davis et al., 2016). This suggests that, besides the induction of feedback regulation, thylakoid $\Delta\Psi$-dissipating channels have an important function for the avoidance of PSII damage.

The fraction of pmf stored as $\Delta\Psi$ can be increased by another thylakoid ion transport mechanism, via the K^+ EXCHANGE ANTIPORTER 3 (KEA3; Armbruster et al., 2014; Kunz et al., 2014; Armbruster et al., 2016; Dukic et al., 2019; Wang and Shikanai, 2019). KEA3 exports protons from the lumen in exchange for another cation, most likely K^+ (Armbruster et al., 2014; Tsujii et al., 2019) and thereby decreases the ΔpH fraction of the pmf. Loss of *KEA3* strongly delays NPQ relaxation and thus negatively affects CO_2 assimilation after a transition from high to low light (Armbruster et al., 2014).

[1]This work was funded by a Deutsche Forschungsgemeinschaft (DFG) research grant (AR 808/5-1 to U.A.).

[2]Present address: Institute of Horticulture and Product Physiology, Wageningen University, Droevendaalsesteeg 1, 6700 AA Wageningen, The Netherlands.

[3]Author for contact: armbruster@mpimp-golm.mpg.de.

[4]Senior author.

The author responsible for distribution of materials integral to the findings presented in this article in accordance with the policy described in the Instructions for Authors (www.plantphysiol.org) is: Ute Armbruster (armbruster@mpimp-golm.mpg.de).

V.C.G. performed most of the experiments with help from D.H.; V.C.G., D.D.S., M.A.S., and U.A. interpreted data with help from S. Z.T.; V.C.G. and U.A. analyzed data; M.M., M.W., F.B., and R.H. performed adenylate quantifications; W.T. and M.A.S. quantified thylakoid complexes spectroscopically, measured 77K chlorophyll-a fluorescence emission spectra, cyt-*f* redox state, and performed Chl *a* fluorescence light response curves; S.B. and P.J. performed the pigment analysis; E.K. carried out the CO_2 assimilation measurement; B.S. and B.A.M. performed MS analysis on thylakoid proteins; U.A. wrote the manuscript with help from all authors; U.A. designed the study together with D.D.S. and M.A.S.

[OPEN]Articles can be viewed without a subscription.

www.plantphysiol.org/cgi/doi/10.1104/pp.19.01561

Plants overexpressing *KEA3* instead exhibit faster NPQ relaxation (Armbruster et al., 2016). Additionally, *kea3* mutants were reported to have higher NPQ in steady state at low and medium light intensities, whereas KEA3 overexpressors had lower NPQ (Wang and Shikanai, 2019). In high light, there was little difference in pmf composition and NPQ between plants with different KEA3 levels (Armbruster et al., 2014; Armbruster et al., 2016; Wang and Shikanai, 2019). The overexpression of a KEA3 version lacking its C terminus, which contains a predicted regulatory domain, however, resulted in plants with decreased NPQ in high light. This finding strongly suggested that KEA3 activity is inhibited in high light via a mechanism involving its C terminus (Armbruster et al., 2016). Upon transition from high to low light, KEA3 becomes readily activated as seen by the clear effect that different KEA3 levels have on NPQ relaxation. The identification of KEA3 as an important factor for rapid NPQ relaxation suggested that cpATP synthase activity must be insufficient to quickly down-regulate the lumenal proton concentration and thus NPQ during a high to low light transition (Armbruster et al., 2014). Here, activation of KEA3 and thereby increased partitioning of pmf in $\Delta\Psi$ is required for optimal CO_2 fixation. In the current work, we set out to determine the stoichiometry of KEA3 and cpATP synthase in the thylakoid membrane in Arabidopsis. In addition, we altered KEA3 and cpATP synthase levels by knocking out or overexpressing *KEA3* in the *conserved only in the green lineage160* (*cgl160*) mutant, which lacks a cpATP synthase assembly factor and thus accumulates only 20% of wild-type cpATP synthase (Rühle et al., 2014; Fristedt et al., 2015). This allowed us to address whether the reduced ΔpH component of the pmf previously reported for multiple cpATP synthase limited mutants (Rott et al., 2011; Fristedt et al., 2015; Davis et al., 2016) is KEA3-dependent and beneficial for their photosynthesis and growth.

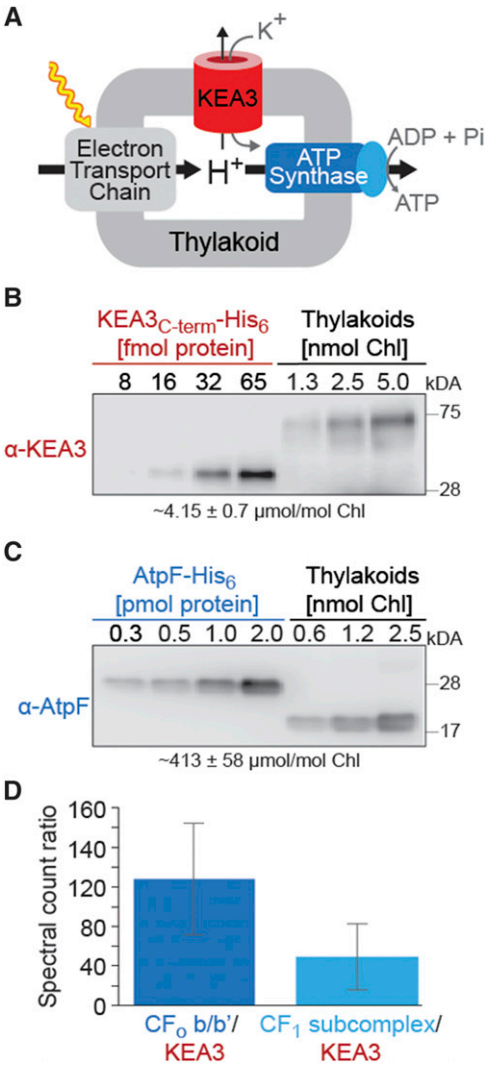

Figure 1. KEA3 occurs substoichiometrically to the cpATP synthase in the thylakoid membrane. A, Scheme depicting the thylakoid membrane with the main proton transport pathways (i.e. the electron transport chain and the ATP synthase, as well as KEA3). B and C, Representative blots of KEA3 (B) and AtpF (C) quantifications obtained by titrating known amounts of purified recombinant proteins, i.e. the C terminus of KEA3 (which binds the specific epitope antibody, Armbruster et al., 2014) and full-length AtpF, against known amounts of thylakoid membranes (quantified by Chl content). Values derived from the quantifications are given below the blots as average of $n = 5 \pm$ SD. D, Ratio of spectral counts identified by MS analysis for the CF_o cpATP b/b′ subunits and the CF_1 cpATP synthase subcomplex with KEA3. Average of $n = 5 \pm$ SD is displayed.

RESULTS

KEA3 Is Much Less Abundant in Thylakoid Membranes than the ATP Synthase

While photosynthetic electron transport reactions generate pmf by depositing protons in the lumen, the majority of protons leave the lumen via the cpATP synthase (Fig. 1A). Both the protein complexes belonging to the pmf-generating electron transport chain, and the pmf-utilizing cpATP synthase are highly abundant and make up a large fraction of the protein content in the thylakoid membrane (Kirchhoff et al., 2002). Proton export from the lumen via KEA3 markedly contributes to increases in the lumenal pH right after high to low light transitions and in steady state at low and medium light intensities (Armbruster et al., 2014; Armbruster et al., 2016; Wang and Shikanai, 2019). KEA3 probably replaces protons with another cation, likely K^+, and thereby decreases the ΔpH component of the pmf (see scheme in Fig. 1A).

To obtain information about the stoichiometric relationship of the proton-transporting mechanisms mediated by the cpATP synthase and KEA3, we titrated thylakoid membranes from the wild type against heterologously expressed and purified KEA3 soluble C terminus and ATP synthase CF_o subunit b (AtpF) with

C-terminal His tags (Fig. 1, B and C). We chose AtpF as a membrane integral subunit (b-subunit of CF_o) of the thylakoid membrane, unlikely to be lost during thylakoid isolation. From the quantifications obtained by protein blot analyses, we calculated an average abundance in thylakoid membranes of about 4.15 μmol/mol chlorophyll (Chl) for KEA3 (Fig. 1B), and 413 μmol/mol Chl for AtpF (Fig. 1C). This makes about 100 cpATP synthase complexes per KEA3 monomer. In an orthogonal approach, thylakoid membranes from the wild type were subjected to mass spectrometry (MS) analysis and spectral count ratios were calculated for each replicate (Fig. 1D). By this method, we obtained an average CF_o-ATP synthase subcomplex to KEA3 ratio of 120 to 1 and a CF_1-ATP synthase subcomplex to KEA3 ratio of 60:1. The lower amount of CF_1 as compared with CF_o suggests that some of this membrane associated subcomplex was lost during thylakoid isolation. Together, these analyses demonstrate that KEA3 occurs substoichiometrically to the photosynthetic complexes in the thylakoid membrane and that the cpATP synthase is about 100-fold more abundant than KEA3.

The *cgl160* Mutant Shows Decreased Membrane Conductivity and ATP Content, But a Strong Increase in Light-Induced pmf

We set out to analyze the effects that loss of KEA3 has on photosynthesis and growth in a mutant with low cpATP synthase content. Here, we chose the *cgl160* mutant, which accumulates 20% of wild-type cpATP synthase levels due to a deficiency in cpATP synthase assembly (Rühle et al., 2014; Fristedt et al., 2015). The proton conductivity of the thylakoid membrane (g_{H^+}), which serves as a proxy for the capacity of the cpATP synthase for proton efflux from the lumen, and the ECS_t parameter, which is a measure of the light induced total pmf, had been determined by monitoring the decay of the electrochromic shift (ECS) during a short dark interval (Fristedt et al., 2015). This analysis revealed that *cgl160* plants have slightly increased light-induced total pmf and decreased g_{H^+}, compared with the corresponding wild type (Col-0). However, the previous experiments had only been performed at saturating light intensities (Fristedt et al., 2015).

To understand how different light intensities affect thylakoid proton conductivity and *pmf* in the *cgl160* mutant, we performed ECS measurements of the wild type and the two previously published *cgl160* mutants at different actinic light intensities. Plants were grown in a 16-h light/8-h dark photoperiod at 150 μmol photons m^{-2} s^{-1} and showed the previously reported reduction in plant size (Fig. 2A; Rühle et al., 2014; Fristedt et al., 2015). Analysis of the ECS decay kinetics revealed that both *cgl160* mutants had a significantly lower g_{H^+} at growth light intensity, which was reduced by 12% to 14% compared with Col-0 (Fig. 2B). The decrease in g_{H^+} as compared with Col-0 was stronger when actinic light intensities were increased (Fig. 2B) and was accompanied by a strong increase in light-induced pmf as expressed by the ECS_t parameter (Fig. 2C). Under actinic light intensities resembling growth light, ECS_t was increased 2.5-fold in both *cgl160* mutants compared with the wild type. Particularly, under intermediate light intensities (150-300 μmol photons m^{-2} s^{-1}), ECS_t of the *cgl160* mutants was more than double the size of Col-0 (Fig. 2C). While in Col-0 light-induced ECS_t increased with actinic light intensities up to 1000 μmol photons m^{-2} s^{-1}, ECS_t in *cgl160* reached its peak at 600 μmol photons m^{-2} s^{-1}. Additionally, we determined whole leaf ATP content in Col-0 and *cgl160* plants. In this analysis, both *cgl160* lines showed reduced levels of ATP as compared with Col-0 (Fig. 2D; Supplemental Table S1). Taken together, our analyses demonstrate that *cgl160* mutants have lower ATP synthase conductivity at growth light. This results in

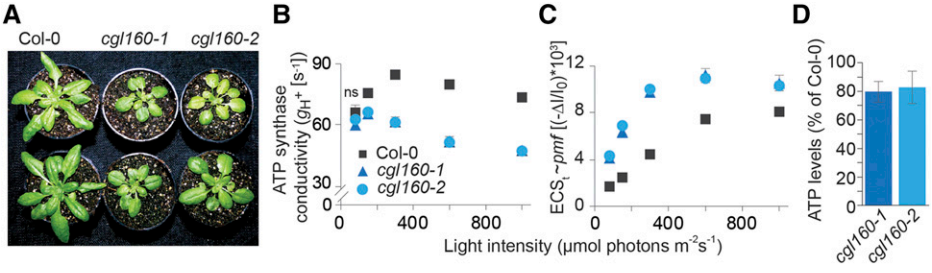

Figure 2. The low cpATP synthase mutant *cgl160* has decreased ATP synthase activity, lower ATP levels, and high pmf. A, Picture of 5-week-old Col-0, *cgl160-1*, and *cgl160-2*. B and C, Membrane proton conductivity (g_{H^+}) as proxy for ATP synthase activity (B) and light-induced thylakoid pmf estimated by ECS_t (C) were calculated from changes in the ECS signal during a short dark interval following 10 min of actinic light illumination at the indicated light intensities. Averages of $n = 6$ are shown and error bars indicate ± SE. ANOVA and a Holm-Sidak pairwise multiple comparison describe g_{H^+} of both mutants to be significantly lower than that of Col-0 ($P < 0.05$), except where stated ns for nonsignificant. For ECS_t, the tests describe mutants to have significantly higher values at all light intensities as compared with Col-0. D, ATP levels of Col-0 and *cgl160-1* or *cgl160-2* were determined from leaf discs in two independent experiments as described in Supplemental Table S1, and ratios between Col-0, *cgl160-1* or *cgl160-2* were calculated.

higher *pmf* and lower ATP levels as compared with the wild type.

In the *cgl160* Background, KEA3 Is Important for Plant Growth by Increasing the Capacity for Photosynthesis

In order to analyze the role of KEA3 in a mutant with low cpATP synthase levels, we generated multiple *cgl160 kea3* double mutants, *cgl160-1 kea3-1*, *cgl160-1 kea3-2*, and *cgl160-2 kea3-1*. Two previously published *kea3* mutants (Armbruster et al., 2014; Kunz et al., 2014; Armbruster et al., 2016; Wang et al., 2017; Dukic et al., 2019; Wang and Shikanai, 2019) showed wild-type–like appearance under our standard growth condition of a 16-h light/8-h dark photoperiod with 150 μmol photons m^{-2} s^{-1} (Fig. 3A). In the *cgl160* background, lack of *KEA3* as in the three *cgl160 kea3* double mutants, caused a much stronger growth defect than lack of *CGL160* alone (Fig. 3A). While 5-week-old Col-0 and *kea3* plants accumulated 12–22 mg of biomass and the *cgl160* mutants accumulated 9–15 mg of biomass, the *cgl160 kea3* double mutants showed a further reduction in growth capacity and accumulated only 5–11 mg of biomass (Fig. 3B).

To further characterize the growth of the mutants, we measured increases in leaf area over time for Col-0, *kea3-1*, *cgl160-1*, and the corresponding *kea3-1 cgl160-1* double mutant and calculated the growth rate. Again, this analysis showed that the *kea3* mutant grows similarly to the wild-type Col-0 (Fig. 3C). The growth rate of the *cgl160* mutant was lower and after 5 weeks *cgl160* mutants showed a reduction in leaf area by ~30% as compared with Col-0 (Fig. 3C). The growth rate and leaf area of *cgl160-1 kea3-1* double mutants were even further reduced with the leaf area

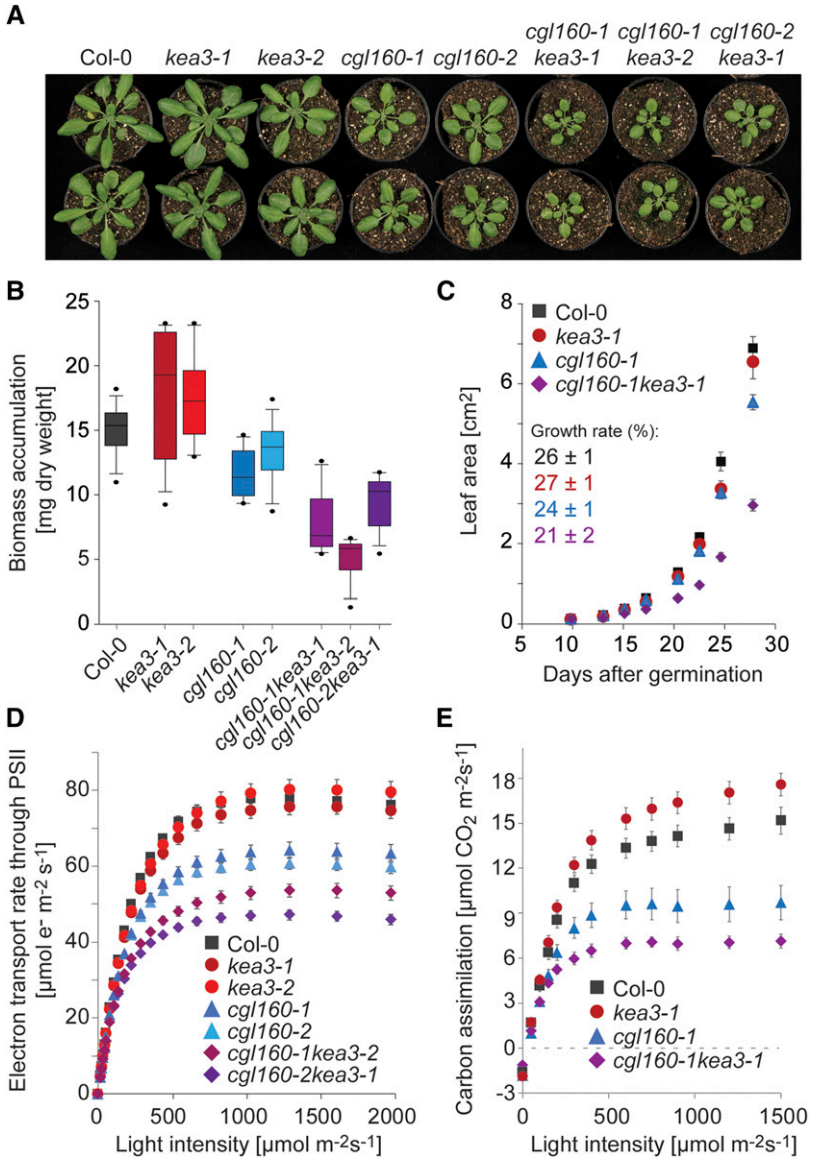

Figure 3. KEA3 optimizes growth in the *cgl160* mutant by increasing the capacity for photosynthesis. A, Picture of 5-week-old Col-0, *kea3-1*, *kea3-2*, *cgl160-1*, *cgl160-2*, *cgl160-1 kea3-1*, *cgl160-1 kea3-2*, and *cgl160-2 kea3-1* plants. B, Dry weight of 5-week-old plants represented as box plots, $n = 13$. C, Increases in leaf area during 5 weeks for Col-0, *kea3-1*, *cgl160-1*, and *cgl160-1 kea3-1*; averages of $n = 6–8$ are shown, and error bars indicate ± SE. The inset shows daily growth rate ± SD (D) Chl *a* fluorescence was measured of dark acclimated plants at increasing actinic light intensities, and the electron transport rate through PSII (ETRII) was calculated; averages of $n = 18$ are displayed and error bars indicate ± SE. E, Whole plant assimilation was determined in response to increasing light intensities and recalculated on a leaf area basis; averages of $n = 7–13$ plus error bars for ± SE are shown.

only reaching ~50% of that of the *cgl160* mutants (Fig. 3C).

To characterize the photosynthetic performance of the plants, we measured Chl *a* fluorescence light response curves and calculated the capacity for linear electron transport. Again, this analysis showed that *kea3* mutants behaved like Col-0 (Fig. 3D). As previously described, *cgl160* mutants (Rühle et al., 2014; Fristedt et al., 2015) exhibited reduced capacity for linear electron transport. The electron transport rate (ETR) was even further decreased in the absence of KEA3 in both independent *cgl160 kea3* mutants (Fig. 3D). Particularly, at light intensities >100 and <1000 μmol photons m^{-2} s^{-1}, *cgl160 kea3* double mutants displayed a much stronger reduction in ETR as compared with *cgl160* alone. Light response curves of whole plant CO_2 assimilation were performed with Col-0, *kea3-1*, *cgl160-1*, and *cgl160-1 kea3-1* and confirmed the reduced capacity of the *cgl160* mutants for photosynthesis, which was even further decreased in the absence of KEA3 in the *cgl160-1 kea3-1* mutant (Fig. 3E). Taken together, these data show that loss of KEA3 alone does not have a strong effect on growth and photosynthesis in the steady state, when plants are grown under low light conditions. *cgl160* mutants, as previously reported, have a lower capacity for photosynthesis and growth (Rühle et al., 2014; Fristedt et al., 2015). Lack of KEA3 in the *cgl160* background further decreases the capacity of these plants to perform steady-state photosynthesis and thus negatively affects growth. This shows that *cgl160* plants require KEA3 for optimal photosynthesis and thereby biomass accumulation.

cgl160 Mutants Store a Large Fraction of pmf as $\Delta\Psi$ in a KEA3-Dependent Manner

Proton antiport by KEA3 shifts the pmf composition toward higher $\Delta\Psi$ and lower ΔpH, while not markedly altering the overall size of the light-induced pmf (Armbruster et al., 2014; Kunz et al., 2014; Dukic et al., 2019; Wang and Shikanai, 2019). Additionally, plants with a low cpATP synthase content and/or activity, including the *cgl160* mutant, store a larger fraction of pmf as $\Delta\Psi$ (Kohzuma et al., 2009; Rott et al., 2011; Fristedt et al., 2015; Davis et al., 2016). To analyze the size of light-induced pmf and its composition in ΔpH and $\Delta\Psi$ of Col-0, *kea3*, *cgl160*, and *cgl160 kea3* plants under our growth conditions, we monitored the ECS signal at growth light (150 μmol photons m^{-2} s^{-1}) and during relaxation in a prolonged dark period (Fig. 4A; Sacksteder et al., 2000; Cruz et al., 2001). The ECS signal rapidly decays after transition to dark and the extent of this decay gives information about the total size of the light induced pmf (ECS_t). The ECS then recovers to a steady-state signal in the dark. The difference between the ECS signal in the light and steady state in darkness is referred to as ECS_{ss} and corresponds to the fraction of *pmf* stored as $\Delta\Psi$, whereas the difference between the minimum ECS signal and steady-state dark, which is referred to as ECS_{inv}, corresponds to the pmf fraction stored as ΔpH (Fig. 4A; Cruz et al., 2001). For Col-0 and *kea3* plants at growth light, an ECS_t transmittance signal of around $1.5 * 10^{-3}$ was measured (Fig. 4B) to which ECS_{ss} and ECS_{inv} contributed equally (Fig. 4, A and B). The *cgl160* and *cgl160 kea3* mutants, at growth light, had much higher ECS_t values of around $4 * 10^{-3}$, with little difference between the two genotypes (Fig. 4, A and B). In the *cgl160* mutant, only 32% of the ECS signal corresponded to ECS_{inv}, supporting the previous finding that *cgl160* mutants store a larger fraction of their pmf as $\Delta\Psi$ and less as ΔpH (Fristedt et al., 2015). Instead, the *cgl160 kea3* double mutants had a significantly larger ECS_{inv} amplitude (i.e. ΔpH), making up about 45% of the ECS_t. This result strongly suggests that at least part of the high $\Delta\Psi$ fraction of pmf in the *cgl160* mutants is KEA3 dependent. cpATP synthase conductivity (g_{H^+}) was not affected by loss of KEA3, only by loss of CGL160 (Fig. 4C). Additionally, we calculated the halftime ($t_{1/2}$) of the recovery of the ECS_{inv} phase. This parameter was recently shown to correlate negatively with KEA3 levels at light intensities where KEA3 is active (Wang and Shikanai, 2019). No differences were observed between Col-0, *kea3*, and *cgl160*; however, $t_{1/2}$ was slightly, but not significantly, increased in the double mutants (Supplemental Fig. S1A). Taken together, the ECS results demonstrate that *cgl160 kea3* mutants, with their increased storage of *pmf* as ΔpH, have a much lower lumenal pH than *cgl160* mutants, suggesting that this may cause increased feedback down-regulation of photosynthesis and thus a reduced capacity to photosynthesize and grow. In order to investigate this hypothesis in detail, we performed multiple analyses that monitor lumen-pH related characteristics of the photosynthetic electron transport chain (Fig. 4D). We performed these analyses by using actinic light that simulated the growth light intensity.

Loss of KEA3 in the *cgl160* Background Exacerbates Low pH-Dependent Quenching and Photosynthetic Control

As discussed before, a high proton concentration in the lumen triggers feedback down-regulation of photosynthesis by increasing qE and the de-epoxidation state of xanthophylls (DEPS), and slowing down electron transfer via the Cyt b_6f complex (Hager, 1969; Nishio and Whitmarsh, 1993; Niyogi et al., 1998; Takizawa et al., 2007). Changes in the rate of PQH_2 oxidation can be estimated from the redox states of both the PSII acceptor side (qL, corresponding to PSII acceptor availability) and cytochrome f of the Cyt b_6f complex (cyt-*f*), as well as the PSI donor side (Y[ND]; Fig. 4D). Alterations in pmf composition may also affect PSII function, as it has been shown that a high membrane potential increases PSII charge recombinations and thus photoinhibitory quenching (qI; Davis et al., 2016).

Our analyses performed at growth light intensities showed that none of the genotypes differed with

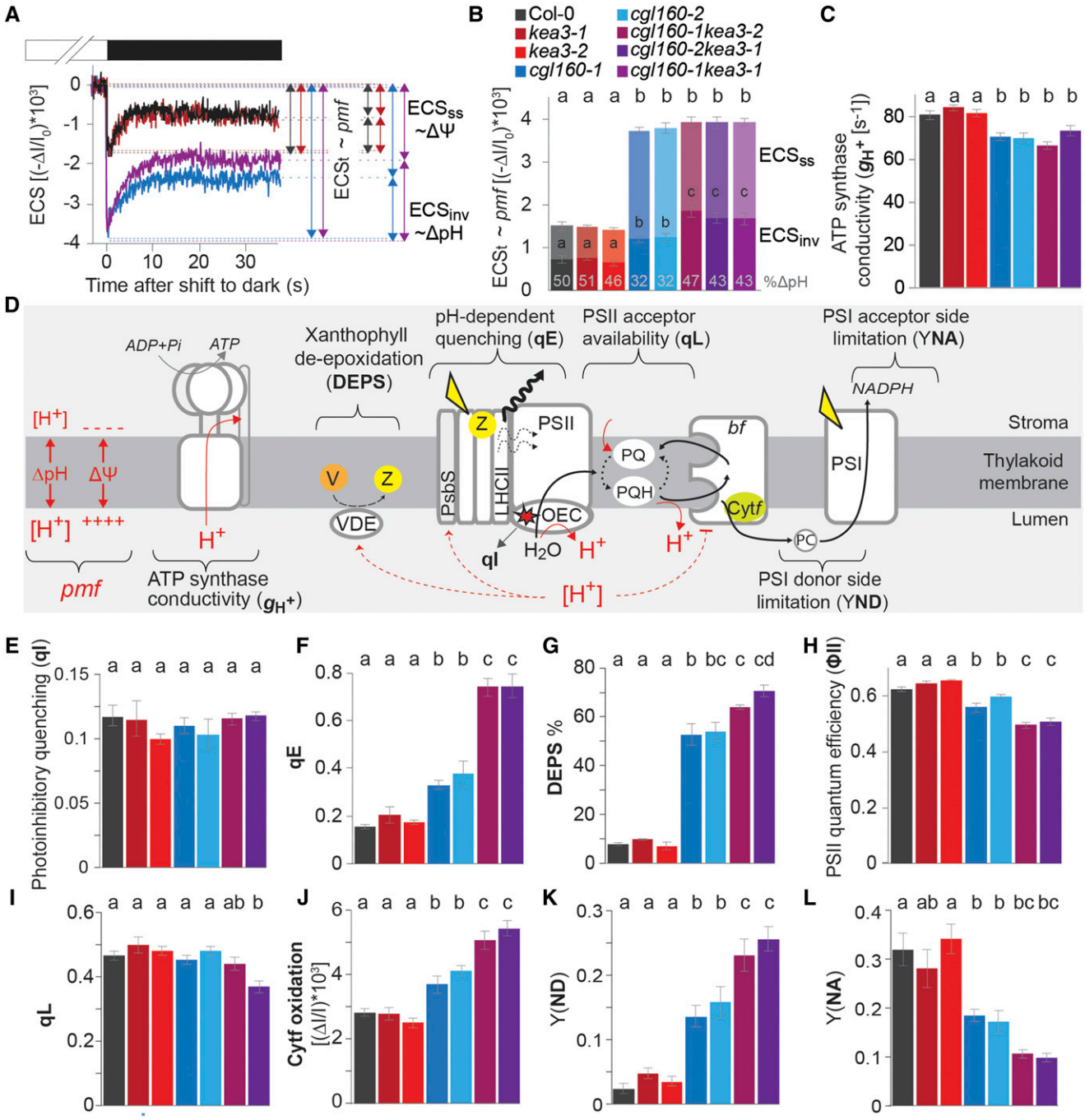

Figure 4. In the *cgl160* mutant, KEA3 decreases the ΔpH component of the pmf and thereby increases photosynthetic electron transport. A and B, At growth light, the *cgl160* mutant stores a high fraction of pmf as ΔΨ, which is KEA3-dependent. Representative ECS traces of Col-0, *kea3-1*, *cgl160-1*, and *kea3-1 cgl160-1* plants during a transition from light (150 μmol photons m^{-2} s^{-1}) to dark (A). The difference in the ECS signal between light and the transient minimum in dark is ECS_t, between light and steady-state dark ECS_{ss} and between transient dark minimum and steady-state dark ECS_{inv}. ECS_t is a measure for light induced pmf, ECS_{ss} for ΔΨ and ECS_{inv} for ΔpH. B, ECS and its composition measured for Col-0, *kea3-1*, *kea3-2*, *cgl160-1*, *cgl160-2*, *cgl160-1 kea3-1*, *cgl160-1 kea3-2*, and *cgl160-2 kea3-1*. Averages are shown for $n = 10$, and error bars indicate ± SE. Different letters above and in graph indicate significant differences between genotypes with $P < 0.05$ as determined by ANOVA and a Holm-Sidak pairwise multiple comparison for ECS_t and ECS_{inv}, respectively. C, Membrane conductivity for protons (g_{H^+}). D, Scheme of the thylakoid membrane depicting the composition of the pmf, the regulatory role of the lumenal proton concentration, and parameters that were derived in this work. VDE, violaxanthin de-epoxidase; V, violaxanthin; Z, zeaxanthin; LHCII, light harvesting complex II; OEC, oxygen evolving complex; PQ, plastoquinone; *bf*, cytochrome b_6f complex; PC, plastocyanin. E to L, photoinhibitory quenching (qI, E), pH-dependent quenching (qE, F and indicated as curvy black arrow in D), xanthophyll deepoxidation

respect to photoinhibitory quenching (qI; Fig. 4E). Also, the wild-type and both *kea3* mutants did not differ significantly in any of the other measured parameters (Fig. 4, F–L). For *cgl160* mutants, qE and DEPS were significantly increased as compared with Col-0 and *kea3* (Fig. 4, F and G). This finding is in line with the larger ECS_{inv} signal, suggesting lower lumenal pH in the *cgl160* mutants as compared with Col-0 (Fig. 4B). Whereas PSII efficiency (ΦII) was decreased in the *cgl160* mutants (Fig. 4H), qL was comparable with Col-0 (Fig. 4I). However, cyt-*f* oxidation was significantly increased by about 30%, and PSI donor side limitation was approximately six times higher in both *cgl160* mutants as compared with Col-0 (Fig. 4, J and K). Additionally, PSI acceptor side limitation was decreased by ~50% (Fig. 4L). In nearly all cases, alterations in photosynthetic parameters measured for the *cgl160* mutants as compared with Col-0 and *kea3* were more strongly affected in the *cgl160 kea3* mutants (Fig. 4, F–L). Both independent *cgl160 kea3* double mutants showed a two-fold increase in qE as compared with their *cgl160* parents (Fig. 4F), and DEPS was increased by ~20% (Fig. 4G), which again is in line with the larger ECS_{inv} signal in the *cgl160 kea3* mutants as compared with the *cgl160* mutants (Fig. 4B). ΦII was also significantly reduced (Fig. 4H). qL was only lower in *cgl160-2 kea3-1*, but not in *cgl160-1 kea3-2* as compared with the other genotypes (Fig. 4I).

A stronger inhibition of PQ oxidation was evident from the cyt-*f* oxidation measurement, which showed that the *cgl160 kea3* mutants had a 25% higher cyt-*f* oxidation as compared with the *cgl160* mutants (Fig. 4J). The amplitude changes of the cyt-*f* transmission signal, when measured at saturating light, were indistinguishable between genotypes (Supplemental S1B), supporting that the difference at growth light intensity stemmed from a higher relative oxidation level of cyt-*f*. PSI donor side limitation Y(ND) was increased by ~50% in the *cgl160 kea3* mutants as compared with the *cgl160* mutants (Fig. 4K), whereas PSI acceptor side limitation Y(NA) was not significantly different from the single mutants (Fig. 4L). We also analyzed leaf adenylates and showed that lack of KEA3 in the *cgl160* background did not change leaf ATP levels (Supplemental S1, C and D).

Loss of KEA3 in the *cgl160* Mutant Is Associated with a Decrease in Plastocyanin Content

Except for the cpATP synthase, thylakoid complexes in the *cgl160* mutant accumulate at wild-type levels (Rühle et al., 2014; Fristedt et al., 2015). Also, lack of KEA3 does not affect thylakoid complex content (Armbruster et al., 2014). To investigate whether the thylakoid composition was different in *cgl160 kea3* mutants as compared with the other genotypes, we analyzed pigment levels, quantified PSII, Cyt b_6f, plastocyanin (PC), and PSI spectroscopically and performed immunoblot analyses (Fig. 5). No clear difference in Chl per leaf area could be demonstrated between genotypes except for *kea3-1* and *cgl160-2 kea3-1* (Fig. 5A). Additionally, no strong differences between genotypes were observed for PSII, Cyt b_6f, and PSI content, when normalized to Chl and leaf area (Fig. 5, B–D; Supplemental Table S2). Interestingly, the *cgl160-1 kea3-2* double mutant showed significantly lower PC content as compared with its *cgl160-1* parent, when levels were normalized to Chl (Fig. 5E). When calculated on a leaf area basis, PC was reduced in both *cgl160 kea3* lines as compared with each of their two parents by ~20% (Fig. 5F).

To verify these findings, we performed protein blot analyses on total protein extracts by using specific antibodies. We probed total protein extracts from Col-0, *kea3-1*, *cgl160-1* and the double mutant with antibodies specific for KEA3 and CGL160 (Fig. 5G). The results clearly showed that CGL160 and KEA3 were present at wild-type levels in the *kea3* and *cgl160* mutants, respectively, but lacking in the corresponding mutants. Additionally, we probed total leaf protein with the AtpB antibody that recognizes the CF_1 β-subunit of the cpATP synthase. This analysis confirmed the decrease in cpATP synthase in both the *cgl160* and *cgl160 kea3* mutants to levels < 25% of the wild type, as shown previously (Rühle et al., 2014; Fristedt et al., 2015). Levels of PsbS, which is known to determine the amplitude of energy pH-dependent quenching (Niyogi et al., 1998; Li et al., 2002), were not changed between genotypes. Protein blot analyses corroborated our spectroscopic quantification results: Levels of complexes from the photosynthetic electron transport chain were determined by using specific antibodies for PsbA (D1-subunit of PSII), PetA (cyt-*f* subunit of Cyt b_6f) and PsaB (B subunit of PSI) and showed few differences between genotypes (Fig. 5G). Only PC content was again measurably reduced in the *cgl160 kea3* mutants to about 75% of the other genotypes.

Additional pigment analyses suggested some minor remodeling of the protein complex composition in the thylakoid membrane in the *cgl160 kea3* mutants as compared with the wild type. The Chl a/b ratio was slightly, but significantly lower in the *cgl160 kea3* mutants as compared with Col-0 and the two *kea3* mutants, while the Chl a/b ratio for the *cgl160* mutant was between that of wild type and the *cgl160 kea3* mutants, but

Figure 4. (*Continued.*)
state (DEPS, G), PSII quantum efficiency (ΦII, H), PSII acceptor availability (qL, I), cyt-*f* oxidation state (J), PSI donor side limitation (Y[ND]; K), and PSI acceptor side limitation (Y[NA] L). Average is shown for $n = 10$ (C, E, F, H) and $n = 6–8$ (G and I–L), and error bars indicate ± SE. A–C and E–L, Measurements were performed on 5-week-old plants at actinic light intensities resembling growth light as described in "Materials and Methods." Different letters above bars indicate significant differences between genotypes with $P < 0.05$ as calculated by ANOVA and Holm-Sidak pairwise multiple comparison (C and E–L).

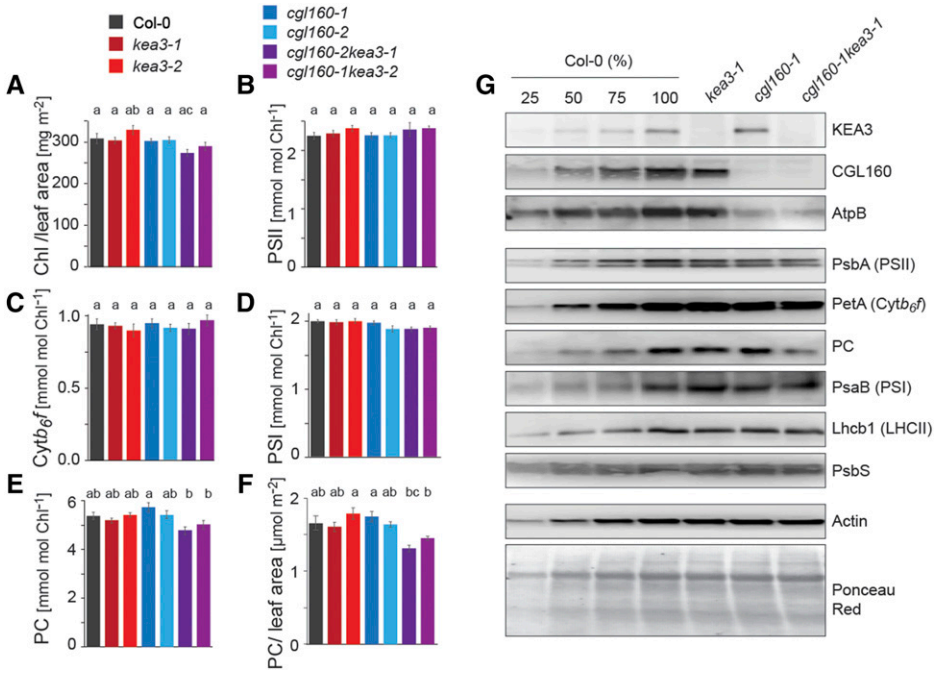

Figure 5. In the *cgl160* mutant, lack of KEA3 decreases plastocyanin content. A, Chl content per leaf area is very similar between 5-week-old Col-0, *kea3-1*, *kea3-2*, *cgl160-1*, *cgl160-2*, *cgl160-1kea3-2*, and *cgl160-2kea3-1* plants. B to F, PSII (B), Cytb_6f (C), PSI (D), and PC (E) were quantified spectroscopically with respect to Chl in isolated thylakoids as described in the methods. F, PC per leaf area was calculated from data in (A) and (E). Averages are shown for $n = 6$, and error bars indicate ± SE. Different letters above bars indicate significant differences between genotypes with $P < 0.05$ as calculated by ANOVA and post hoc Tukey's test. Note that PC per leaf area for *cgl160-1kea3-2* and *cgl160-2kea3-1* is significantly different from both parents, *cgl160-1*, *kea3-2* and *cgl160-2*, *kea3-1*, respectively. G, Western blot analysis of total leaf protein from Col-0 (dilution series), *kea3-1*, *cgl160-1*, and *cgl160-1kea3-1* with antibodies as indicated on the right. Before immune detection, membranes were stained with Ponceau Red.

not significantly altered as compared with either (Table 1). However, no changes were found in the PSI/PSII ratio as calculated from the spectroscopic quantification of each complex (Supplemental Table S2). This was corroborated by unaltered levels of β-carotene, a pigment more abundant in PSI, between *cgl160 kea3* and Col-0 (Table 1). Also, levels of neoxanthin, which only binds to the antenna of PSII, were similar between genotypes. Together with western blot results from the light harvesting complex b1 (Lhcb1) antibody showing no difference between genotypes, this strongly suggests that the size of the PSII antenna remained unchanged (Table 1).

Only lutein, which binds all antenna proteins, was significantly higher in the *cgl160 kea3* mutants as compared with Col-0 (Table 1). The VAZ pool, which is the sum of the xanthophylls violaxanthin, antheraxanthin and zeaxanthin, was significantly increased in *cgl160* mutants compared with Col-0, as shown previously (Rühle et al., 2014), and was even further, but not significantly increased in both *cgl160 kea3* mutants. Additionally, the relative antenna cross sections of the

Table 1. *Pigments from Col-0,* kea3*,* cgl160*, and* cgl160kea3 *Plants*

Pigments were extracted and quantified as described in "Materials and Methods." Values for neoxanthin, lutein, carotene, violaxanthin + antheraxanthin + zeaxanthin are given in millimole per mole Chl. The Chl a/b ratio was calculated, and PSI/PSII is derived from the spectroscopic quantification shown in Figure 5. Average values ($n = 5$) and standard deviations are provided. The letters indicate the results from ANOVA and post hoc Tukey's test.

Genotype	Chl a/b	Carotene	Neoxanthin	Lutein	Violaxanthin
Col-0	2.96 ± 0.17 a,b	63.2 ± 1.4 a,b	26.4 ± 0.9 a	88.9 ± 4.2 a	28.3 ± 2.1 a
kea3-1	3.03 ± 0.07 a	63.5 ± 2.6 a,b	27.9 ± 1.3 a	101.4 ± 7.5 a,b	41.9 ± 4.3 a,b
kea3-2	3.06 ± 0.02 a	64.0 ± 3.1 a	27.1 ± 1.5 a	96.8 ± 8.2 a,b	39.5 ± 5.5 a,b
cgl160-1	2.83 ± 0.05 b	58.7 ± 3.8 b	27.3 ± 0.9 a	102.4 ± 7.2 a,b	51.3 ± 9.8 b
cgl160-2	2.83 ± 0.03 b,c	62.6 ± 2.5 a,b	25.6 ± 1.0 a	95.1 ± 6.9 a,b	49.8 ± 7.5 b
cgl160-1kea3-2	2.70 ± 0.02 b,c	58.4 ± 1.8 b	27.6 ± 0.9 a	107.5 ± 7.2 b	60.9 ± 7.8 b,c
cgl160-2kea3-1	2.65 ± 0.03 c	59.0 ± 2.5 a,b	25.4 ± 1.3 a	109.2 ± 7.0 b	69.1 ± 9.8 c

photosystems were determined from 77K Chl *a* fluorescence emission spectra (Supplemental Fig. S2). No changes in the ratio of the emission signals of PSII-LHCII peaking at 687 nm wavelength and PSI-LHCI peaking at 733 nm wavelength were observed, supporting that antenna cross sections and excitation distribution between the photosystems were unchanged between genotypes.

Loss of *cgl160* Increases High Light Sensitivity

Previously, it was shown that high $\Delta\Psi$ favors charge recombination within PSII (Davis et al., 2016; Davis et al., 2017) and that low lumenal pH below 5.5 triggers the release of calcium from the oxygen evolving complex (Krieger and Weis, 1993). Both high $\Delta\Psi$ and low lumen pH can thus increase the slowly relaxing photoinhibitory quenching component qI that accompanies PSII damage (Krause and Weis, 1991). However, when we analyzed Col-0, *kea3*, *cgl160*, and *cgl160 kea3* for qI under actinic light intensities resembling growth light, no differences were observed (Fig. 4E). These results suggested that if PSII damage was increased in *cgl160* and *cgl160 kea3* mutants as compared with the other genotypes under growth light, it did not exceed the capacity of the plants for PSII repair. This finding was corroborated by measurements of the maximum quantum yield of PSII, Fv/Fm, which was also unchanged between genotypes (Fig. 6A).

Plants were then challenged with light stress by exposing them to six times the growth light intensity (900 μmol photons m^{-2} s^{-1}) for 3 h: all genotypes showed a significant decrease in Fv/Fm after the high light treatment, but it was more severe in *cgl160* plants independent of whether they were additionally lacking KEA3 (Fig. 6A). In order to analyze the link between *pmf* composition and PSII photoinhibition, we determined light induced *pmf* (ECS_t) and its composition, ΔpH (ECS_{inv}), and $\Delta\Psi$ (ECS_{ss}) of plants after 15 min of high light. This analysis showed that all genotypes had a very similar ECS_{ss} independent of the size of ECS_t, which in turn was higher in plants lacking *cgl160* (Fig. 6B). This could indicate that the size of $\Delta\Psi$ is regulated to remain below a certain threshold, potentially to avoid $\Delta\Psi$-induced PSII charge recombination. The results also suggest that at high light KEA3 does not influence the composition of pmf, which is in line with previous publications (Armbruster et al., 2016; Wang and Shikanai, 2019), not even in the *cgl160* background.

Overexpression of *KEA3* in the *cgl160* Background Further Decreases qE But Not Photosynthetic Control

Because we observed that *cgl160* mutants require KEA3 for efficient photosynthesis and growth, we investigated whether we could improve photosynthesis and growth by overexpressing the major KEA3 isoform *KEA3.2* in the *cgl160* background. Therefore, we transformed *cgl160-1* plants with a construct to overexpress a KEA3.2-GFP fusion, which was previously shown to complement *kea3* mutant phenotypes, when expressed at wild-type level (Armbruster et al., 2014). We isolated two lines, which showed a more than 4-fold overexpression of KEA3-GFP compared with *cgl160-1*, which will be referred to *as oeKEA3$_{cgl160}$* (Supplemental Fig. S3). The oeKEA3$_{cgl160}$ plants had strongly decreased cpATP synthase levels similar to those of the *cgl160* mutants, which was determined by Western blot analysis of total protein by using the AtpB antibody (Supplemental Fig. S3). *oeKEA3$_{cgl160}$* plants looked slightly larger than *cgl160-1* plants, but still much

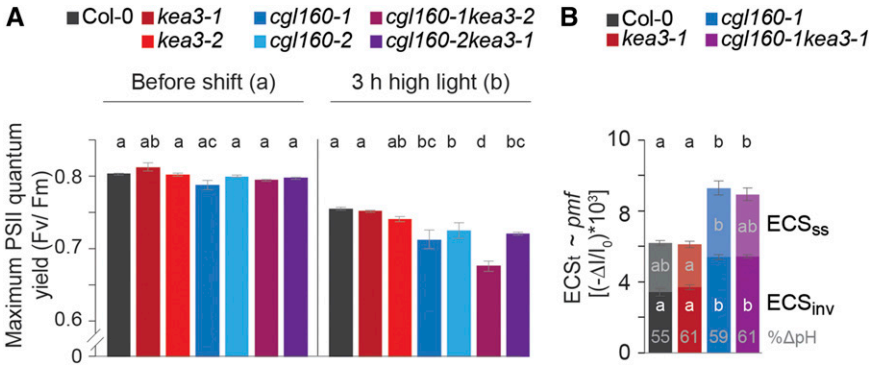

Figure 6. *cgl160* plants are sensitive to high light independent of KEA3. A, Maximum quantum yield of 5-week-old Col-0, *kea3-1*, *kea3-2*, *cgl160-1*, *cgl160-2*, *cgl160-1 kea3-2*, and *cgl160-2 kea3-1* was measured before and 3 h after a shift to 900 μmol photons m^{-2} s^{-1}. Averages are shown for $n = 10$, and error bars indicate ± SE. Different letters above bars indicate significant differences between genotypes with $P < 0.05$ as calculated by ANOVA and post hoc Tukey's test. B, Light-induced pmf (ECS_t) and fraction stored as $\Delta\Psi$ (ECS_{ss}) and ΔpH (ECS_{inv}) was measured at 1000 μmol photons m^{-2} s^{-1} actinic light for Col-0, *kea3-1*, *cgl160-1*, and *cgl160-1 kea3-1*. Average is shown for $n = 5$, and error bars indicate ± SE. Different letters above graph indicate significant differences between genotypes for ECS_t, in top bar for ECS_{ss} and in bottom bar for ECS_{inv} with $P < 0.05$ as calculated by ANOVA and post hoc Tukey's test.

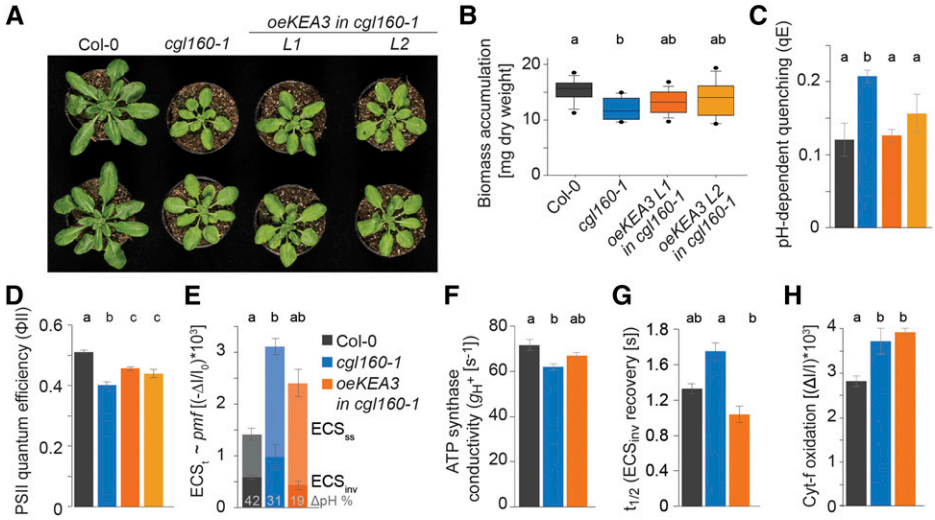

Figure 7. Overexpression of *KEA3* in the *cgl160* background promotes photosynthesis by down-regulating qE. A, Picture of 5-week-old Col-0, *cgl160-1* and two independent lines overexpressing KEA3-GFP in the *cgl160-1* background. B, Dry weight of 5-week-old plants; $n = 13–15$. Different letters above graph indicate significant differences between genotypes with $P < 0.05$ as calculated by ANOVA on ranks and Dunn's test (C and D) pH-dependent quenching (qE; C) and PSII quantum efficiency (ΦII; D) were measured of Col-0, *cgl160-1*, and *oeKEA3* lines 1 and 2 (L1 and L2) in the *cgl160-1* background. Averages are shown for $n = 6$, and error bars indicate ± SE. E to H, Light-induced pmf (ECS_t) and fraction stored as ΔΨ (ECS_{ss}) and ΔpH (ECS_{inv}; E), cpATP synthase conductivity (g_{H^+}; F), halftime ($t_{1/2}$) of ECS_{inv} recovery (G), and cyt-*f* oxidation state (H) were measured for Col-0, *cgl160-1*, *oeKEA3 in cgl160-1* L1 and L2. Data for both overexpression lines were pooled for representation and statistical analysis. Average is shown for $n = 3–10$, and error bars indicate ± SE. C to H, Measurements were performed at actinic light intensities resembling growth light as detailed in "Materials and Methods." Different letters above graph indicate significant differences between genotypes with $P < 0.05$ as calculated by ANOVA and Holm-Sidak pairwise multiple comparison.

smaller than Col-0 (Fig. 7A). While *cgl160-1* mutants accumulated significantly less dry weight than Col-0, the dry weight of the two KEA3 overexpression lines was between that of Col-0 and *cgl160-1*, and not significantly different from either (Fig. 7B).

Then we measured Chl *a* fluorescence and ECS based parameters at actinic light intensities resembling growth light (Fig. 7, C–G). Chl *a* fluorescence analysis demonstrated that *KEA3* overexpression in the *cgl160-1* background lowers pH-dependent quenching (qE) to levels comparable with Col-0 (Fig. 7C). This decrease in qE was accompanied by a significant increase in PSII efficiency (ΦII) in both $oeKEA3_{cgl160}$ lines as compared with *cgl160-1* (Fig. 7D). We determined ECS_t, ECS_{ss}, and ECS_{inv} to analyze the effect of high KEA3 levels on light induced pmf and its composition in the *cgl160-1* background (Fig. 7E). This analysis showed that $oeKEA3_{cgl160}$ had more light-induced pmf stored as ΔΨ compared with Col-0 and *cgl160-1*. However, differences were not significant. Interestingly, while ECS_t was much higher in *cgl160-1* as compared with Col-0 (as was also shown in Figs. 2C and 4B), ECS_t was reduced in the overexpressors to levels that were not significantly different from the wild type (Fig. 7E). The membrane conductivity for protons (g_{H^+}) behaved in the opposite way, that is, while g_{H^+} in *cgl160-1* was significantly decreased as compared with Col-0, overexpression of KEA3 in $oeKEA3_{cgl160}$ resulted in g_{H^+} values that were in between Col-0 and *cgl160-1*, not significantly different to either (Fig. 7F). The halftime of ECS_{inv} recovery ($t_{1/2}$) tended to be higher in *cgl160-1* than in the wild type, but this difference was not significant. However, overexpression of *KEA3* further reduced $t_{1/2}$ to levels significantly lower than those in *cgl160-1* (Fig. 7G).

Interestingly, cyt-*f* oxidation, which was increased significantly in *cgl160-1* compared with Col-0 (as was also shown for *cgl160-2* in Fig. 4J) was not further changed by overexpression of *KEA3-GFP* (Fig. 7H; Supplemental Table S3). Additionally, the thylakoid complex composition was analyzed spectroscopically, and no significant differences were found between Col-0, *cgl160-1*, and $oeKEA3_{cgl160}$ (Supplemental Table S4). Together, the data indicate that overexpression of *KEA3* in the *cgl160* background may pose an advantage for photosynthesis and growth. The results clearly demonstrate that higher KEA3 levels decrease pH-dependent quenching, increase PSII efficiency, and accelerate ECS_{inv} recovery in the *cgl160-1* background.

DISCUSSION

Photosynthesis and Growth of the *cgl160* Plants, with Low cpATP Synthase Content, Benefit from KEA3 Activity

Previously, photosynthetic phenotypes of *kea3* mutants and *KEA3* overexpressors were described. It was

shown that KEA3 decreases the ΔpH component of the pmf and thereby downregulates NPQ (Armbruster et al., 2014; Kunz et al., 2014; Armbruster et al., 2016; Wang et al., 2017; Dukic et al., 2019; Wang and Shikanai, 2019). The main function of KEA3 is in intermediate light conditions and during transition from high to low light (Armbruster et al., 2014; Dukic et al., 2019; Wang and Shikanai, 2019). However, so far lack of *KEA3* or overexpression of naturally occurring KEA3 isoforms has not been associated with a strong effect on growth.

In the current work, we set out to analyze the influence that the absence or overexpression of *KEA3* has in the *cgl160* mutant, which has strongly reduced cpATP synthase levels (<25% of wild type (Rühle et al., 2014; Fristedt et al., 2015; Fig. 5G). We could show that in this background, KEA3-mediated proton export from the lumen promotes growth, that is, *cgl160 kea3* mutants accumulate less biomass than *cgl160* single mutants (Fig. 3, A–C). In the *cgl160* mutant, with high *pmf*, KEA3 enables higher photosynthesis rates by down-regulating energy-dependent quenching (qE) and up-regulating the rate of plastoquinol oxidation at the Cyt b_6f complex (i.e. decreasing photosynthetic control; Fig. 4). Together, the data demonstrate that photosynthesis in *cgl160 kea3* mutants is limited by low electron transport rates as a result of a high ΔpH.

In *cgl160* single mutants instead, KEA3 counteracts the high lumenal proton concentration by converting ΔpH into ΔΨ and thereby upregulates photosynthesis. Interestingly, while levels of all other protein components of the electron transport chain remained unchanged between genotypes, PC content was reduced in mutants that lacked both *CGL160* and *KEA3*. In the *cgl160 kea3* mutants, PC may either be directly destabilized by low lumenal pH, as previously suggested (Kramer et al., 1999), or decreased by mechanisms at the transcriptional or posttranscriptional level. Many mutants affected in photosynthesis instead up-regulate PC content, starting at the transcriptional level in response to starvation signals (i.e. low sugar; Oswald et al., 2001; Schöttler et al., 2004; Rott et al., 2011). Hence, the reduction in PC content in the *cgl160 kea3* mutants is unlikely to be a response to the decrease in assimilation capacity we observed in this double mutant, because in this case we would expect the opposite, that is, an increase in PC content. Thus, it appears plausible that PC content may be indeed sensitive to lumenal pH.

Regardless of the mechanism by which PC content is decreased, the question remains of whether the low PC content contributes to the decrease in photosynthesis observed in the *cgl160 kea3* mutants. A substantial decrease in PC content can result in PC being rate-limiting for photosynthesis (Schöttler et al., 2004). At such low PC levels, PSI would be strongly donor side limited and cyt-*f* of Cyt b_6f more reduced (Schöttler et al., 2004). However, cyt-*f* is more oxidized in the *cgl160 kea3* mutants (Fig. 4J), which points to PQ oxidation and not PC reduction being the rate-limiting step at Cyt b_6f in this background.

The Regulation of pmf Composition by KEA3 Affects the Rate of Plastoquinol Oxidation at Cyt b_6f

The increased oxidation level of cyt-*f* and PSI (Fig. 4) in the *cgl160* mutants and even more strongly in the *cgl160 kea3* double mutants suggest that electron transport from PQ via cyt-*f* to PSI (i.e. the high potential chain) is slowed down at growth light intensity due to lower Cyt b_6f turnover. An alternative explanation for increased oxidation of cyt-*f* and PSI could be imbalanced excitation rates of the photosystems, so that PSI is excited in excess and thereby oxidizes the high potential chain. This alternative explanation is unlikely, because neither photosynthetic complex contents nor antenna cross sections of the photosystems were altered (Fig. 5; Supplemental Fig. S2). Thus, the higher cyt-*f* oxidation in the *cgl160 kea3* mutants compared with the *cgl160* mutants strongly supports a role for KEA3-dependent proton antiport in alleviating photosynthetic control, at least in the *cgl160* background.

Recent work by Wang and Shikanai (Wang and Shikanai, 2019) interpreted a decrease in PSI donor side limitation (Y[ND]) in *KEA3* overexpressors as compared with wild type as a result of increased Cyt b_6f turnover. In the present work, we show by measurement of the cyt-*f* redox state that overexpression of *KEA3* does not increase Cyt b_6f turnover in the *cgl160* background (Fig. 7). Thus, while lack of *KEA3* in the *cgl160* mutants increases both qE and photosynthetic control (Fig. 4), *KEA3* overexpression in the *cgl160* mutants only downregulates qE (Fig. 7H). Together, these data support the notion that qE and Cyt b_6f turnover are affected differently by high pmf.

While the main determinant of qE seems to be the net proton concentration in the lumen, which behaves inversely to KEA3 levels in the *cgl160* background (Figs. 4B and 7E), photosynthetic control appears not only to be dependent on ΔpH, but also on ΔΨ. This is in line with thermodynamic considerations and results obtained with the homologous mitochondrial bc1 complex, which show that collapsing the membrane potential increases the rate of electron transport through this complex (Rich and Clarke 1982). However, the strong increase in cyt-*f* oxidation seen in the *cgl160 kea3* mutants as compared with the *cgl160* mutants supports an additional kinetic down-regulation of Cyt b_6f turnover by low lumenal pH, possibly due to the protonation of amino acids involved in proton transfer from the plastoquinol binding site to the lumen (Tikhonov, 2014).

KEA3 Activity Is Tightly Regulated

KEA3 activity changes the composition of the pmf toward higher ΔΨ. KEA3 may achieve this either directly by increasing the membrane potential through electrogenic antiport, for example, if it transports multiple K^+ per proton, and/or indirectly by dissipating the ΔpH component, thus forcing a larger fraction of

pmf to be stored as $\Delta\Psi$. The exact transport mechanism of KEA3 has yet to be determined. Our results demonstrate KEA3 to be present in thylakoid membranes at much lower levels than the cpATP synthase and, therefore, at first sight may question a direct competition of KEA3 with the cpATP synthase for proton export from the lumen (Fig. 1). However, maximum proton transport rates for antiporters can be much higher than those for the cpATP synthase: The *Escherichia coli* Na+/H+ antiporter A (NhaA), which belongs to the same class of cation proton antiporter2 (CPA2) transporters as KEA3 (Masrati et al., 2018) has been shown to have a maximum turnover rate of 9×10^4 s^{-1} (Taglicht et al., 1991). At high pmf, a maximum ATP synthesis rate of ~400 ATP s^{-1} per protein complex has been reported (Gräber et al., 1987). In line with a ~4.7 H^+/ 1 ATP stoichiometry (Petersen et al., 2012), one cpATP synthase complex could achieve a maximum proton transport rate of ~ 1.9×10^3 protons s^{-1}. Assuming an equally high maximum activity for KEA3 as reported for NhaA, this would imply that one KEA3 has the same maximum proton transport capacity as 50 cpATP synthases. With ~100 cpATP synthases per KEA3, proton export from the lumen by KEA3 could reach at least 50% of the cpATP synthase, assuming no kinetic or thermodynamic constraints on each of the two transport processes.

Proton transport via KEA3 could be thermodynamically limited by low concentrations of the antiported cation. However, stromal concentrations of free K^+ are in the millimolar range (discussed in Cruz et al., 2001) and thereby in excess of the lumenal proton concentration. While K^+ has been shown be transported by KEA3 (Tsujii et al., 2019), a high selectivity for K^+ has not yet been unequivocally demonstrated. Also, other cations, such as Na^+ and Mg^{2+}, are present at concentrations exceeding the micromolar range (Robinson and Downton, 1984; Ishijima et al., 2003). Thus, exchange of the entire ΔpH with a cation concentration gradient should be feasible through KEA3. This clearly does not occur. Therefore, proton export from the lumen via KEA3 must be kinetically controlled, either by a lower affinity of KEA3 for the antiported ions as compared with NhaA or via regulation of its activity.

KEA3 activity has been shown to be regulated via its C terminus (Armbruster et al., 2016). This C terminus contains a conserved K+ transport nucleotide-binding domain, which in other systems gates K^+ transport in response to nucleotide binding (Choe, 2002; Roosild et al., 2002; Cao et al., 2013; Kim et al., 2015). The two main products of the light reactions of photosynthesis, ATP and NADPH, have been shown to strongly decrease in response to a high to low light transition (Stitt et al., 1989), the very condition where an activation of KEA3 occurs (Armbruster et al., 2016). Thus, it is tempting to speculate that KEA3 is activated in response to lower levels of one or both of these nucleotides or an increase in ADP or $NADP^+$, their low energy counterparts.

Activation by low ATP or high ADP may explain why we see such a strong effect of KEA3 on pmf composition specifically in the *cgl160* mutant with decreased ATP levels (Fig. 2D). However, the strong effect that loss of KEA3 has in the *cgl160* background on pmf composition can be alternatively explained by the following: (1) low proton transport rates through the cpATP synthase, because of its low content, and/or (2) high rates of proton efflux via KEA3 because of high pmf. However, both explanations predict that further increases of pmf, for example, by high light, would exacerbate the effect that KEA3 has on pmf composition in the *cgl160* background. This is, however, not the case, as the difference in pmf composition between the *cgl160* and *cgl160 kea3* mutants collapses in high light (Fig. 6B). This strongly suggests that also in the *cgl160* background KEA3 gets inactivated in high light.

Dissipation of pmf via Simultaneous Activity of KEA3 and a Counterion Channel?

One interesting observation is that overexpression of *KEA3* in the *cgl160* background causes significantly reduced light-induced pmf (as demonstrated by the ECS_t parameter), while absence of *KEA3* does not affect the pmf size. One possible explanation for this is the simultaneous activity of KEA3 and the corresponding thylakoid cation (likely K^+) channel in the *cgl160* background, when KEA3 is overexpressed. Together, both would be cycling K^+ with net efflux of protons from the lumen and thus dissipate pmf. In the *cgl160* mutant, K^+ channel activity must be much lower than that of KEA3, because we do observe a strong effect on pmf composition (i.e. higher $\Delta\Psi$ in *cgl160* than in *cgl160 kea3*), which should not be present if both antiporter and channel had the same ion transport capacity. However, if we speculate that the K^+ channel is voltage gated, the membrane potential may reach a critical threshold in the $oeKEA3_{cgl160}$ line at which the K^+ channel is activated and together with KEA3 starts dissipating pmf.

Is there any evidence that the thylakoid K^+ channel is voltage gated? First of all, the function of thylakoid counter ion channels such as the K^+ channel is the dissipation of $\Delta\Psi$, and thus it is intuitive that these channels should be activated by high $\Delta\Psi$. Multiple studies have reported on the presence of a K^+ channel in the thylakoid membrane by electrophysiological approaches (Tester and Blatt, 1989; Enz et al., 1993; Pottosin and Schönknecht, 1996), and indeed in one study a moderate voltage dependence of the channel was described (Pottosin and Schönknecht, 1996). However, so far, the molecular nature of the thylakoid K^+ channel and thus its regulation remains unknown (Höhner et al., 2019). The only thylakoid counter-ion channel that has convincingly been shown to reside in the thylakoid membrane is the Cl^- channel VCCN1, and this is in fact voltage-gated (Duan et al., 2016; Herdean et al., 2016). Besides lower pmf size, the $oeKEA3_{cgl160}$ plants also displayed significantly faster ECS_{inv} recovery (Fig. 7). The recovery phase of the ECS signal in the dark (ECS_{inv}) occurs after proton

flux from the lumen has caused the generation of an inverse membrane potential.

Two mechanisms can explain the phenomenon of the ECS recovery: slow ion flux that collapses the inverse membrane potential (Cruz et al., 2001) or proton flux from the stroma into the lumen by the cpATP synthase (Szabò and Spetea, 2017). Previously, the acceleration of ECS_{inv} by KEA3 has been shown to correlate with an increase in the parameter g_{H^+}, which reflects the proton conductivity of the thylakoid membrane and has been used to describe cpATP synthase activity (Wang and Shikanai, 2019). This correlation was used to support that KEA3 transport activity causes increases in g_{H^+}. We also see a slight increase in g_{H^+} in the oeKEA3$_{cgl160}$ line as compared with the *cgl160* mutant. However, how and whether these two parameters are directly correlated remains to be determined.

CONCLUSIONS

This study aimed at characterizing the functional interaction of two exit routes for protons from the thylakoid lumen, that is, the cpATP synthase and the proton antiporter KEA3, on the physiological level. Hereby, we could show that in a mutant with low cpATP synthase content (i.e. *cgl160*), the presence of KEA3 confers a physiological advantage by decreasing the lumenal proton concentration, which in turn increases the capacity of the *cgl160* mutant for light harvesting and electron transport. This is of physiological significance, because it suggests that under conditions that limit ATP synthase activity, proton transport via KEA3, which functions to increase the fraction of the pmf as $\Delta\Psi$, controls photosynthesis and growth.

MATERIAL AND METHODS

Plant Material, Propagation, and Growth Conditions

The Arabidopsis *(Arabidopsis thaliana) kea3-1* (Gabi_170G09), *kea3-2* (SAIL_556_E12), *cgl160-1* (SALK_057229), and *cgl160-2* (WiscDsLoxHs024_02B) T-DNA insertion lines have been described previously (Armbruster et al., 2014; Kunz et al., 2014; Rühle et al., 2014; Fristedt et al., 2015). The *cgl160 kea3* plants were generated by crossing and identifying double homozygous mutants in the F2 generation by PCR-based genotyping using primers as detailed in Supplemental Table S5. *cgl160-1* plants expressing *KEA3.2-GFP* (*KEA3$_{cgl160}$*) were generated via *Agrobacterium*-mediated floral dip (Clough and Bent, 1998) by using the pB7FWG2-KEA3.2 construct described in Armbruster et al., 2014.

Wild-type Arabidopsis accession Col-0 and transgenic seeds were stratified for 2 d at 4°C in 1% agarose with gibberellic acid A4 and A7 (0.2% and 0.1% [v/v] respectively) to synchronize germination. Seeds were sown on soil, grown in long-day conditions (16-h light/8-h darkness at 20°C/ 6°C, 60%/75% relative humidity) at 250 μmol photons m^{-2} s^{-1} for 7 d. Plants were then moved to long-day conditions with 120-150 μmol photons m^{-2} s^{-1} and 16°C night temperature. After 2 weeks, plants were pricked into individual pots. All measurements were performed with plants that were 4 to 5 weeks old.

Growth and Biomass Accumulation Analysis

The leaf area of whole rosettes was determined by detecting the minimal Chl *a* fluorescence (F_0) under measuring light using the Walz Imaging PAM (Walz GmbH) and quantification using Image J according to Schneider et al., 2012. The increase in leaf area over time was fitted exponentially to derive the daily growth rate. For representation only those plants were selected where the R^2-value of the fit was >0.99. For dry weight measurements, 5-week-old rosettes were harvested and dried for 3 d under vacuum at 65°C.

Expression and Purification of Recombinant KEA3-C Terminus and AtpF Protein

The KEA3 C terminus and AtpF were amplified from complementary DNA by using primers described in Supplemental Table S5 and cloned into the pET28a (+) vector (Novogen). His-tagged KEA3 C terminus (KEA3$_{C\text{-}term}$His$_6$) and AtpF (AtpF-His$_6$) were obtained by using standard protocols for recombinant protein expression and purification using Ni-NTA affinity chromatography. The purity of the recombinant protein was checked on SDS PAGE (SDS-PAGE) stained with Coomassie brilliant blue. The concentrations of the recombinant proteins were determined by Pierce BCA Protein Assay kit (Thermo Scientific).

Mass Spectrometric Identification and Quantification of ATP Synthase and KEA3

Thylakoids resuspended in 8 M urea and 10 mM Tris-HCl (pH 8.0) were reduced with dithiothreitol, modified with iodoacetamide and digested on column with trypsin (Promega) in 100 mM ammonium bicarbonate (ratio trypsin to protein of 1:25 [w/w]). Digest was performed for 14 h at 37°C. Peptides were eluted with 0.5 M NaCl. Trifluoroacetic acid (10% [w/v]) was used for peptide acidification to pH < 3.0. The peptide mixture was purified and desalted on C18 SEP-Pak columns (Tecknokroma). Measurements were performed on a Q Exactive *Plus* combined with HF mass spectrometer coupled with a nLC1000 nano-HPLC (both Thermo Scientific). Quantitative analysis of tandem MS measurements was performed with MaxQuant software (Cox and Mann, 2008), and Mascot search engine was used to annotate peptide sequences using the Arabidopsis TAIR10 genome annotation database. The following settings were used for a search: 10 ppm peptide mass tolerance; 0.8 D tandem MS tolerance; maximum of two missed cleavages allowed, threshold for validation of peptides set to 0.01, carbamidomethylation of Cys was set as a fixed modification and oxidation of Met was set as variable modification. The 'label-free quantification' and 'match between runs' options were selected. The minimum peptide length of six amino acids was used. The quantification was performed for proteins with minimum of one unique and one razor peptide. Known contaminants such as keratins were removed from further analysis.

Nucleotide Quantification

ATP, ADP, and AMP were quantified fluorometrically after specific derivatization with chloroacetaldehyde as described in Bürstenbinder et al., 2007. ATP, ADP, and AMP were quantified fluorometrically after specific derivatization with chloroacetaldehyde as described in Bürstenbinder et al., 2007. Nucleotides were extracted from frozen ground material (20 mg) in 50 μL of 0.1 M HCl using a mixer mill with a zirconia bead for 1 min at 25 Hz, and centrifuged at 16,000 g at 4°C for 10 min. After centrifugation, 15 μL of the supernatant mixed with 77 μL of CP buffer [62 mM citric acid-1hydrate and 76 mM $(Na)_2HPO_4 0.2H_2O$, pH 4] was derivatized by adding 8 μL of 45% (v/v) chloroacetaldehyde for 10 min at 80°C. Separation of derivatized nucleotides was carried out as in Estavillo et al., 2011 using a HyperClone C18 (ODS) column (Phenomenex) on a Summit HPLC system (Dionex). Nucleotide amounts were determined by measuring the area under the curve and calculated based on a calibration curve of derivatized nucleotide standards.

ECS, Chl *a* Fluorescence, and P700 Measurements

Near simultaneous Chl *a* fluorescence and ECS measurements were performed on intact leaves of 30-min dark-adapted plants using a custom-made spectrophotometer (Hall et al., 2013). Plants were illuminated for 10 min at various light intensities (Fig. 2, B and C), 150 μmol photons m^{-2} s^{-1} (Figs. 4, A and B, and 7, E–G–G), and 1000 μmol photons m^{-2} s^{-1} (Fig. 7) to reach steady state. The dark interval relaxation kinetics (DIRK) of the 520 nm ECS signal monitored for 300 ms was used to estimate thylakoid proton conductivity (g_{H^+}) by fitting the ECS decay curve to a first order exponential, and the amplitude of the dark-light signal to estimate ECS_t (light-induced thylakoid pmf) as previously described (Kanazawa and Kramer, 2002). DIRKs for three wavelengths (505, 520, and 535 nm) were monitored for 40 s, and the ECS signal was

deconvolved as described (Cruz et al., 2001) to determine the amplitude and partitioning of the pmf. The half time ($t_{1/2}$) of the ECS_{inv} recovery signal was calculated by fitting data to the equation $y = A_1*e^{(x/t1)} + y_0$ using Origin (OriginLab) and settings for orthogonal distance regression. All ECS signals were normalized to the total Chl content of the leaf.

For Chl *a* fluorescence yield measurements, saturation light pulses as in Strand et al., 2017 were applied after dark acclimation (for Fm), steady-state illumination (for Fm′), and 10 min of dark relaxation (for Fm′′). qE and qI components of NPQ were calculated as [(Fm′′− Fm′)/Fm′] and [(Fm − Fm′′)/ Fm′′], respectively. A Dual-PAM-100 instrument (Walz GmbH) was used to measure PSII acceptor availability (qL) and light-dependent electron transport rate through PSII as in Baker, 2008. For P700 measurements, leaves were illuminated for 12 min at 135 μmol photons m^{-2} s^{-1}. Fv/Fm values in Figure 6 were measured using the Imaging PAM (Walz GmbH).

77K Chl *a* fluorescence emission spectra were measured on freshly isolated thylakoid membranes equivalent to 10 μg chlorophyll mL^{-1} using a F-6500 fluorometer with a red-sensitive photomultiplier (Jasco Inc.). The sample was excited at 430-nm wavelength with a bandwidth of 10 nm, and the emission spectrum was recorded between 655- and 800-nm in 0.5-nm intervals with a bandwidth of 1 nm. All signals were normalized to the emission maximum of PSII-LHCII at 686.5 nm wavelength.

Cyt-*f* Oxidation State Measurements

Light-dark difference transmittance signals after 10-min illumination at 111 and 1295 μmol photons m^{-2} s^{-1} followed by 30-s dark in the dark were measured at multiple wavelengths between 505 and 570 nm using a KLAS-100 spectrophotometer (Walz GmbH). Transmittance signals for cyt-*f* were deconvoluted from the ECS signal, scattering, and other cytochromes as previously described (Klughammer et al., 1990; Rott et al., 2011). The deconvoluted redox kinetics of cyt-*f* were normalized to the chlorophyll content of the leaf.

Quantification of Photosynthetic Complexes

PSII, Cyt b_6f, PSI, and PC were quantified spectroscopically in isolated thylakoids extracted as in Schöttler et al., 2004. PSII and Cyt b_6f contents were determined from differences in absorption signals of cyt-b_{559} (PSII) and cyt-*f* and -b_6 (cyt-*bf*). After complete oxidation of all cytochromes by the addition of 1 mM potassium ferricyanid (+III), cyt-*f* and the high-potential form of cyt-b_{559} were reduced by the addition of 5 mM sodium ascorbate, followed by the addition of 10 mM sodium dithionite, to reduce the low-potential form of cyt-b_{559} and the cytochromes b_6. For each redox condition, ten absorbance spectra between 580 and 535 nm wavelength were averaged using a Jasco V-550 photometer equipped with a head-on photomultiplier with a scanning speed of 100 nm * min^{-1} and a spectral bandwidth of 1 nm (Jasco GmbH). Then, differences in absorbance spectra were calculated, baseline-corrected and deconvolved as described (Kirchhoff et al., 2002; Lamkemeyer et al., 2006).

Redox-active PSI content was determined from light-induced absorption changes of P_{700} in the presence of 10 mM sodium ascorbate as the electron donor and methylviologen as the artificial electron acceptor (Schöttler et al., 2007). PC contents, relative to P_{700}, were determined in leaves by in vivo difference absorption spectroscopy in the far-red range of the spectrum and then recalculated based on the absolute P_{700} quantification in isolated thylakoids as described in Schöttler et al., 2007 and finally renormalized to a leaf area basis with the known chlorophyll content per leaf area.

CO_2 Fixation Measurements

Light response curves of net photosynthesis rates were determined using the LI-6400 photosynthesis system (Li-Cor). The soil was covered using parafilm M (Brand) to reduce soil-borne evaporation. Plants were analyzed in the 6400-17 whole plant Arabidopsis chamber, which was equipped with the 6400-18A RGB light source. Measurements were performed at 400 ppm CO_2, 21% O_2, and 55% to 65% relative humidity, 20°C cuvette temperature, and a flow rate of 500 μmol air s^{-1}. Plants were exposed to increasing light intensities up to 1500 μmol m^{-2} s^{-1}. At each light intensity, after steady state was reached, data were logged 10× over a period of 30 s; these data points were averaged for the representation. After the rosette was cut off, soil respiration was determined to correct values. Projected leaf area was determined using ImageJ.

Western Blot Analyses

Total protein was extracted from liquid nitrogen frozen leaf tissue (1 cm^2 diameter leaf disc) in 100 μL 4 × Laemmli buffer as described in Armbruster et al., 2016. Total leaf protein was separated by SDS PAGE and blotted onto a nitrocellulose membrane as in Schwarz et al., 2015. After incubation with specific antibodies—Anti-KEA3 (Armbruster et al., 2014), Anti-PsbS (Correa-Galvis et al., 2016; Correa-Galvis et al., 2016), Anti-Actin (Sigma), and Anti-CGL160, AtpB, PsbA, PetA, PC, PsaB, AtpF and Lhcb1 (Agrisera)—signal was detected by using a C-DiGit Blot Scanner (LI-COR Biosciences).

Pigment Analyses

Total chlorophyll from a 5-mm diameter leaf disc was extracted by the addition of 80% (v/v) acetone and measured according to Porra et al., 1989 for the normalization of ECS and cyt-*f* oxidation signals as well as for data in Figure 5. Additionally, total chlorophyll, xanthophylls, and β-carotene were extracted from 1 cm^2 leaf disc by 1 mL acetone (100%). The supernatant was filtered through a 0.2 μm membrane filter (GE Healthcare). Pigments were separated and quantified by HPLC analysis as previously described (Färber et al., 1997). The DEPS of xanthophylls was calculated as (zeaxanthin + 0.5 anteraxanthin)/ (violaxanthin + anteraxanthin + zeaxanthin).

Statistical Analyses

ANOVAs and Holm-Sidak or Tukey pot hoc tests were performed by using the program SigmaPlot.

Accession Numbers

The following genes and proteins were investigated: *KEA3* (*At4g04850*), *CGL160* (*At2g31040*), AtpB (ATCG00480), PetA (ATCG00540), PsaB (ATCG00340), PsbA (ATCG00020), plastocyanin (PC, AT1G20340, AT1G76100), Lhcb1 (AT1G29910, AT1G29920, AT1G29930, AT2G34420, AT2G34430), and PsbS (AT1G44575). Further information on the mutant lines that were used in the study can be found in the "Material and Methods" section under plant material.

Supplemental Data

The following supplemental materials are available.

Supplemental Figure S1. Spectroscopic data and adenylate quantification.

Supplemental Figure S2. The 77K Chl *a* fluorescence emission spectra support an unaltered antenna distribution between both photosystems in Col-0, *kea3*, *cgl160* and *cgl160 kea3* plants.

Supplemental Figure S3. Western blot analysis of $oeKEA3_{cgl160}$ plants.

Supplemental Table S1. Leaf ATP, AMP and ATP contents of *Col-0*, *cgl160-1* and *cgl160-2*.

Supplemental Table S2. PSII, Cyt b_6f and PSI content per leaf area and PSI/PSII of Col-0, *kea3*, *cgl160* and *cgl160kea3* plants.

Supplemental Table S3. Fv/Fm, qI and Cyt-*f* oxidation of Col-0, *cgl160-1* and $oeKEA3_{cgl160}$.

Supplemental Table S4. Thylakoid complexes are unchanged between Col-0, *cgl160-1* and $oeKEA3_{cgl160}$.

Supplemental Table S5. Primer purpose, names, and DNA sequence used in this study.

ACKNOWLEDGMENTS

We thank Max Blanck, Yvonne Paulenz, and Manjy Thieme at Max Planck Institute of Molecular Plant Physiology Golm for technical support.

Received January 13, 2020; accepted January 27, 2020; published February 10, 2020.

LITERATURE CITED

Allen J (2002) Photosynthesis of ATP-electrons, proton pumps, rotors, and poise. Cell **110:** 273–276

Armbruster U, Carrillo LR, Venema K, Pavlovic L, Schmidtmann E, Kornfeld A, Jahns P, Berry JA, Kramer DM, Jonikas MC (2014) Ion antiport accelerates photosynthetic acclimation in fluctuating light environments. Nat Commun **5:** 5439

Armbruster U, Correa Galvis V, Kunz HH, Strand DD (2017) The regulation of the chloroplast proton motive force plays a key role for photosynthesis in fluctuating light. Curr Opin Plant Biol **37:** 56–62

Armbruster U, Leonelli L, Correa Galvis V, Strand D, Quinn EH, Jonikas MC, Niyogi KK (2016) Regulation and levels of the thylakoid K+/H+ antiporter KEA3 shape the dynamic response of photosynthesis in fluctuating light. Plant Cell Physiol **57:** 1557–1567

Baker NR (2008) Chlorophyll fluorescence: A probe of photosynthesis in vivo. Annu Rev Plant Biol **59:** 89–113

Bürstenbinder K, Rzewuski G, Wirtz M, Hell R, Sauter M (2007) The role of methionine recycling for ethylene synthesis in Arabidopsis. Plant J **49:** 238–249

Cao Y, Pan Y, Huang H, Jin X, Levin EJ, Kloss B, Zhou M (2013) Gating of the TrkH ion channel by its associated RCK protein TrkA. Nature **496:** 317–322

Carraretto L, Formentin E, Teardo E, Checchetto V, Tomizioli M, Morosinotto T, Giacometti GM, Finazzi G, Szabó I (2013) A thylakoid-located two-pore K+ channel controls photosynthetic light utilization in plants. Science **342:** 114–118

Choe S (2002) Potassium channel structures. Nat Rev Neurosci **3:** 115–121

Clough SJ, Bent AF (1998) Floral dip: A simplified method for Agrobacterium-mediated transformation of Arabidopsis thaliana. Plant J **16:** 735–743

Correa-Galvis V, Poschmann G, Melzer M, Stühler K, Jahns P (2016) PsbS interactions involved in the activation of energy dissipation in Arabidopsis. Nat Plants **2:** 15225

Cox J, Mann M (2008) MaxQuant enables high peptide identification rates, individualized p.p.b.-range mass accuracies and proteome-wide protein quantification. Nat Biotechnol **26:** 1367–1372

Cruz JA, Sacksteder CA, Kanazawa A, Kramer DM (2001) Contribution of electric field ($\Delta\ \psi$) to steady-state transthylakoid proton motive force (pmf) in vitro and in vivo. control of pmf parsing into $\Delta\ \psi$ and Δ pH by ionic strength. Biochemistry **40:** 1226–1237

Davis GA, Kanazawa A, Schöttler MA, Kohzuma K, Froehlich JE, Rutherford AW, Satoh-Cruz M, Minhas D, Tietz S, Dhingra A, Kramer DM (2016) Limitations to photosynthesis by proton motive force-induced photosystem II photodamage. eLife **5:** e16921

Davis GA, Rutherford AW, Kramer DM (2017) Hacking the thylakoid proton motive force for improved photosynthesis: Modulating ion flux rates that control proton motive force partitioning into $\Delta\psi$ and ΔpH. Philos Trans R Soc Lond B Biol Sci **372:** 20160381

Duan Z, Kong F, Zhang L, Li W, Zhang J, Peng L (2016) A bestrophin-like protein modulates the proton motive force across the thylakoid membrane in Arabidopsis. J Integr Plant Biol **58:** 848–858

Dukic E, Herdean A, Cheregi O, Sharma A, Nziengui H, Dmitruk D, Solymosi K, Pribil M, Spetea C (2019) K^+ and Cl^- channels/transporters independently fine-tune photosynthesis in plants. Sci Rep **9:** 8639

Dunkel M, Latz A, Schumacher K, Müller T, Becker D, Hedrich R (2008) Targeting of vacuolar membrane localized members of the TPK channel family. Mol Plant **1:** 938–949

Enz C, Steinkamp T, Wagner R (1993) Ion channels in the thylakoid membrane (a patch-clamp study). Biochim Biophys Acta Bioenerg **1143:** 67–76

Estavillo GM, Crisp PA, Pornsiriwong W, Wirtz M, Collinge D, Carrie C, Giraud E, Whelan J, David P, Javot H, Brearley C, Hell R, et al (2011) Evidence for a SAL1-PAP chloroplast retrograde pathway that functions in drought and high light signaling in Arabidopsis. Plant Cell **23:** 3992–4012

Färber A, Young AJ, Ruban AV, Horton P, Jahns P (1997) Dynamics of Xanthophyll-Cycle activity in different antenna subcomplexes in the photosynthetic membranes of higher plants (the relationship between zeaxanthin conversion and nonphotochemical fluorescence quenching). Plant Physiol **115:** 1609–1618

Fristedt R, Martins NF, Strenkert D, Clarke CA, Suchoszek M, Thiele W, Schöttler MA, Merchant SS (2015) The thylakoid membrane protein CGL160 supports CF1CF0 ATP synthase accumulation in *Arabidopsis thaliana*. PLoS One **10:** e0121658

Gräber P, Junesch U, Thulke G (1987) The chloroplast ATP-synthase: The rate of the catalytic reaction. *In* J Biggins, ed, Progress in Photosynthesis Research: Volume **3**. Springer Netherlands, Dordrecht, pp 177–184

Hager A (1969) Light dependent decrease of the pH-value in a chloroplast compartment causing the enzymatic interconversion of violaxanthin to zeaxanthin; relations to photophosphorylation. Planta **89:** 224–243

Hall CC, Cruz J, Wood M, Zegarac R, DeMars D, Carpenter J, Kanazawa A, Kramer D (2013) Photosynthetic measurements with the idea spec: An integrated diode emitter array spectrophotometer/fluorometer. In T Kuang, C Lu, and L Zhang, eds, Photosynthesis Research for Food, Fuel and the Future Advanced Topics in Science and Technology in China. Springer, Berlin, Heidelberg, Berlin, pp 184–188

Herdean A, Teardo E, Nilsson AK, Pfeil BE, Johansson ON, Ünnep R, Nagy G, Zsiros O, Dana S, Solymosi K, et al (2016) A voltage-dependent chloride channel fine-tunes photosynthesis in plants. Nat Commun **7:** 11654

Hind G, Nakatani HY, Izawa S (1974) Light-dependent redistribution of ions in suspensions of chloroplast thylakoid membranes. Proc Natl Acad Sci USA **71:** 1484–1488

Höhner R, Galvis VC, Strand DD, Völkner C, Krämer M, Messer M, Dinc F, Sjuts I, Bölter B, Kramer DM, Armbruster U, Kunz HH (2019) Photosynthesis in arabidopsis is unaffected by the function of the vacuolar K^+ channel TPK3. Plant Physiol **180:** 1322–1335

Ishijima S, Uchibori A, Takagi H, Maki R, Ohnishi M (2003) Light-induced increase in free Mg^{2+} concentration in spinach chloroplasts: Measurement of free Mg^{2+} by using a fluorescent probe and necessity of stromal alkalinization. Arch Biochem Biophys **412:** 126–132

Kanazawa A, Kramer DM (2002) In vivo modulation of nonphotochemical exciton quenching (NPQ) by regulation of the chloroplast ATP synthase. Proc Natl Acad Sci USA **99:** 12789–12794

Kim H, Youn SJ, Kim SO, Ko J, Lee JO, Choi BS (2015) Structural studies of potassium transport protein KtrA regulator of conductance of K+ (RCK) C domain in complex with cyclic diadenosine monophosphate (c-di-AMP). J Biol Chem **290:** 16393–16402

Kirchhoff H, Mukherjee U, Galla HJ (2002) Molecular architecture of the thylakoid membrane: Lipid diffusion space for plastoquinone. Biochemistry **41:** 4872–4882

Klughammer C, Kolbowski J, Schreiber U (1990) LED array spectrophotometer for measurement of time resolved difference spectra in the 530-600 nm wavelength region. Photosynth Res **25:** 317–327

Kohzuma K, Cruz JA, Akashi K, Hoshiyasu S, Munekage YN, Yokota A, Kramer DM (2009) The long-term responses of the photosynthetic proton circuit to drought. Plant Cell Environ **32:** 209–219

Kramer DM, Cruz JA, Kanazawa A (2003) Balancing the central roles of the thylakoid proton gradient. Trends Plant Sci **8:** 27–32

Kramer DM, Sacksteder CA, Cruz JA (1999) How acidic is the lumen? Photosynth Res **60:** 151–163

Krause GH, Weis E (1991) Chlorophyll fluorescence and photosynthesis: The basics. Annu Rev Plant Physiol Plant Mol Biol **42:** 313–349

Krieger A, Weis E (1993) The role of calcium in the pH-dependent control of Photosystem II. Photosynth Res **37:** 117–130

Kunz HH, Gierth M, Herdean A, Satoh-Cruz M, Kramer DM, Spetea C, Schroeder JI (2014) Plastidial transporters KEA1, -2, and -3 are essential for chloroplast osmoregulation, integrity, and pH regulation in Arabidopsis. Proc Natl Acad Sci USA **111:** 7480–7485

Lamkemeyer P, Laxa M, Collin V, Li W, Finkemeier I, Schöttler MA, Holtkamp V, Tognetti VB, Issakidis-Bourguet E, Kandlbinder A, et al (2006) Peroxiredoxin Q of *Arabidopsis thaliana* is attached to the thylakoids and functions in context of photosynthesis. Plant J **45:** 968–981

Li XP, Gilmore AM, Caffarri S, Bassi R, Golan T, Kramer D, Niyogi KK (2004) Regulation of photosynthetic light harvesting involves intrathylakoid lumen pH sensing by the PsbS protein. J Biol Chem **279:** 22866–22874

Li XP, Muller-Moule P, Gilmore AM, Niyogi KK (2002) PsbS-dependent enhancement of feedback de-excitation protects photosystem II from photoinhibition. Proc Natl Acad Sci USA **99:** 15222–15227

Masrati G, Dwivedi M, Rimon A, Gluck-Margolin Y, Kessel A, Ashkenazy H, Mayrose I, Padan E, Ben-Tal N (2018) Broad phylogenetic analysis of cation/proton antiporters reveals transport determinants. Nat Commun **9:** 4205

Nishio JN, Whitmarsh J (1993) Dissipation of the proton electrochemical potential in intact chloroplasts (II. The pH gradient monitored by cytochrome f reduction kinetics). Plant Physiol **101:** 89–96

Niyogi KK, Grossman AR, Björkman O (1998) Arabidopsis mutants define a central role for the xanthophyll cycle in the regulation of photosynthetic energy conversion. Plant Cell **10:** 1121–1134

Oswald O, Martin T, Dominy PJ, Graham IA (2001) Plastid redox state and sugars: Interactive regulators of nuclear-encoded photosynthetic gene expression. Proc Natl Acad Sci USA **98:** 2047–2052

Petersen J, Förster K, Turina P, Gräber P (2012) Comparison of the H^+/ATP ratios of the H^+-ATP synthases from yeast and from chloroplast. Proc Natl Acad Sci USA **109:** 11150–11155

Porra RJ, Thompson WA, Kriedemann PE (1989) Determination of accurate extinction coefficients and simultaneous equations for assaying chlorophylls a and b extracted with four different solvents: Verification of the concentration of chlorophyll standards by atomic absorption spectroscopy. Biochim Biophys Acta Bioenerg **975:** 384–394

Pottosin II, Schönknecht G (1996) Ion channel permeable for divalent and monovalent cations in native spinach thylakoid membranes. J Membr Biol **152:** 223–233

Rich PR, Clarke SD (1982) Reconstitution of cytochrome bc1 complex into lipid vesicles and the restoration of uncoupler sensitivity. FEBS Lett **148:** 54–58

Robinson SP, Downton WJS (1984) Potassium, sodium, and chloride content of isolated intact chloroplasts in relation to ionic compartmentation in leaves. Arch Biochem Biophys **228:** 197–206

Roosild TP, Miller S, Booth IR, Choe S (2002) A mechanism of regulating transmembrane potassium flux through a ligand-mediated conformational switch. Cell **109:** 781–791

Rott M, Martins NF, Thiele W, Lein W, Bock R, Kramer DM, Schöttler MA (2011) ATP synthase repression in tobacco restricts photosynthetic electron transport, CO_2 assimilation, and plant growth by overacidification of the thylakoid lumen. Plant Cell **23:** 304–321

Rühle T, Razeghi JA, Vamvaka E, Viola S, Gandini C, Kleine T, Schünemann D, Barbato R, Jahns P, Leister D (2014) The Arabidopsis protein CONSERVED ONLY IN THE GREEN LINEAGE160 promotes the assembly of the membranous part of the chloroplast ATP synthase. Plant Physiol **165:** 207–226

Sacharz J, Giovagnetti V, Ungerer P, Mastroianni G, Ruban AV (2017) The xanthophyll cycle affects reversible interactions between PsbS and light-harvesting complex II to control non-photochemical quenching. Nat Plants **3:** 16225

Sacksteder CA, Kanazawa A, Jacoby ME, Kramer DM (2000) The proton to electron stoichiometry of steady-state photosynthesis in living plants: A proton-pumping Q cycle is continuously engaged. Proc Natl Acad Sci USA **97:** 14283–14288

Schneider CA, Rasband WS, Eliceiri KW (2012) NIH Image to ImageJ: 25 Years of image analysis. Nat Methods **9:** 671–675

Schöttler MA, Flügel C, Thiele W, Stegemann S, Bock R (2007) The plastome-encoded PsaJ subunit is required for efficient Photosystem I excitation, but not for plastocyanin oxidation in tobacco. Biochem J **403:** 251–260

Schöttler MA, Kirchhoff H, Weis E (2004) The role of plastocyanin in the adjustment of the photosynthetic electron transport to the carbon metabolism in tobacco. Plant Physiol **136:** 4265–4274

Schwarz N, Armbruster U, Iven T, Brückle L, Melzer M, Feussner I, Jahns P (2015) Tissue-specific accumulation and regulation of zeaxanthin epoxidase in Arabidopsis reflect the multiple functions of the enzyme in plastids. Plant Cell Physiol **56:** 346–357

Stiehl HH, Witt HT (1969) Quantitative treatment of the function of plastoquinone in phostosynthesis. Z Naturforsch B **24:** 1588–1598

Stitt M, Scheibe R, Feil R (1989) Response of photosynthetic electron transport and carbon metabolism to a sudden decrease of irradiance in the saturating or the limiting range. Biochim Biophys Acta Bioenerg **973:** 241–249

Strand DD, Livingston AK, Satoh-Cruz M, Koepke T, Enlow HM, Fisher N, Froehlich JE, Cruz JA, Minhas D, Hixson KK, et al (2017) Defects in the expression of chloroplast proteins leads to H_2O_2 accumulation and activation of cyclic electron flow around Photosystem I. Front Plant Sci **7:** 2073

Szabò I, Spetea C (2017) Impact of the ion transportome of chloroplasts on the optimization of photosynthesis. J Exp Bot **68:** 3115–3128

Taglicht D, Padan E, Schuldiner S (1991) Overproduction and purification of a functional Na+/H+ antiporter coded by nhaA (ant) from Escherichia coli. J Biol Chem **266:** 11289–11294

Takizawa K, Cruz JA, Kanazawa A, Kramer DM (2007) The thylakoid proton motive force in vivo. Quantitative, non-invasive probes, energetics, and regulatory consequences of light-induced pmf. Biochim Biophys Acta **1767:** 1233–1244

Tester M, Blatt MR (1989) Direct measurement of k channels in thylakoid membranes by incorporation of vesicles into planar lipid bilayers. Plant Physiol **91:** 249–252

Tikhonov AN (2014) The cytochrome b6f complex at the crossroad of photosynthetic electron transport pathways. Plant Physiol Biochem **81:** 163–183

Tikhonov AN, Khomutov GB, Ruuge EK, Blumenfeld LA (1981) Electron transport control in chloroplasts. Effects of photosynthetic control monitored by the intrathylakoid pH. Biochim Biophys Acta Bioenerg **637:** 321–333

Tsujii M, Kera K, Hamamoto S, Kuromori T, Shikanai T, Uozumi N (2019) Evidence for potassium transport activity of Arabidopsis KEA1-KEA6. Sci Rep **9:** 10040

Voelker C, Schmidt D, Mueller-Roeber B, Czempinski K (2006) Members of the Arabidopsis AtTPK/KCO family form homomeric vacuolar channels in planta. Plant J **48:** 296–306

Wang C, Shikanai T (2019) Modification of activity of the thylakoid H+/K+ antiporter KEA3 disturbs pH-dependent regulation of photosynthesis. Plant Physiol **181:** 762–773

Wang C, Yamamoto H, Narumiya F, Munekage YN, Finazzi G, Szabò I, Shikanai T (2017) Fine-tuned regulation of the K^+ /H^+ antiporter KEA3 is required to optimize photosynthesis during induction. Plant J **89:** 540–553